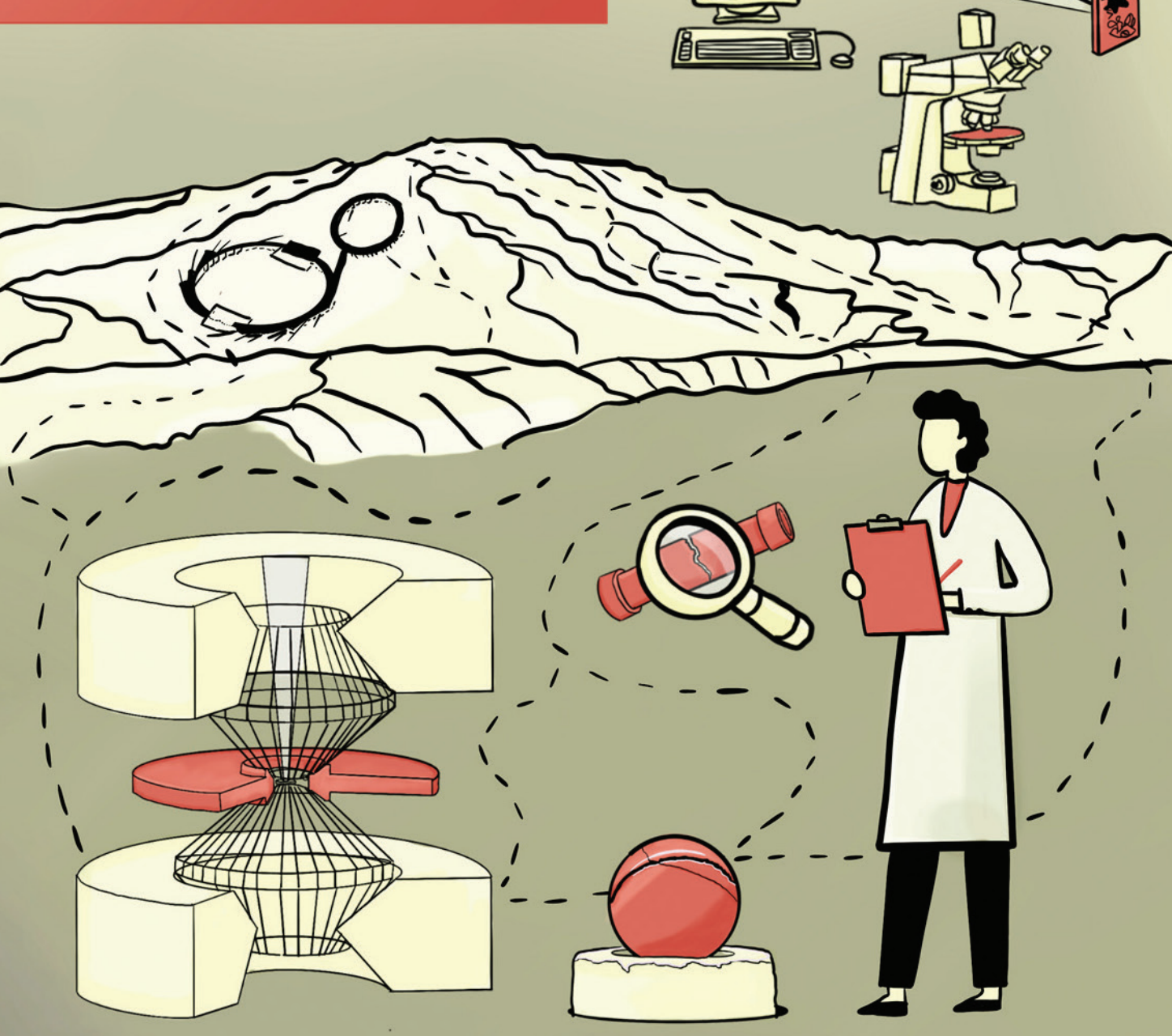
ACTINIDE RESEARCH QUARTERLY

Ac Th Pa U Np Pu Am Cm Bk Cf Es Fm Md No Lr

First Quarter 2025

SEABORG INSTITUTE POSTDOCTORAL ISSUE









Contents





3 Improving Spectroscopic Understanding of Actinides

Joseph Kasper

Probing the Effect of Hydrogen on Uranium

Mary O'Brien

Magnetostriction Studies of Alpha Plutonium

Mark Wartenbe

Actinides Under Extreme Pressures

Larissa Huston

Phosphorus Containing Ligands to Support Variable Oxidation States of *f*-Block Metals

Stephanie Carpenter

Advancing Understanding of Actinides in Aqueous Media

Zach Jones

Actinide Research Quarterly .



Foreword

Los Alamos National Laboratory has remained steadfast in its primary mission of national security for over 80 years but the landscape of challenges it has faced in this period has shifted dramatically, driving its technical evolution. Crucial to this evolution is the science and technology of actinide elements, which is key to all forms of nuclear science. At the core of advancing this field at Los Alamos is the Seaborg Institute, which serves as a catalyst for innovation in actinide science, technology, and engineering. The Institute utilizes LDRD (Laboratory Directed Research and Development) funding to enable the next generation of actinide scientists and engineers, focusing particularly on graduate and postdoctoral researchers. These Seaborg Fellows are integral to ensuring that actinide science continues to thrive at Los Alamos, producing groundbreaking work that also elevates the Laboratory's profile in the global scientific community. In this issue of Actinide Research Quarterly, we showcase the exciting research conducted by several of these exceptional postdoctoral research fellows. Their work spans the diverse and complex world of actinide chemistry, physics, geology, and materials science, whose challenges require access to specialized radiological facilities, advanced diagnostic technologies, and powerful computational tools—resources that are uniquely available within the US Department of Energy's national laboratory complex. Some of the standout projects highlighted in this issue include:

- Joseph Kasper's computational analysis of the electronic structures of actinide complexes. Kasper's high-performance computational work taps into the extraordinary processing power of Los Alamos's supercomputing facilities.
- Mary O'Brien's exploration of how hydrogen influences the thermomechanical properties of uranium. Using the Sigma processing capabilities and the neutron beamline at LANSCE (Los Alamos Neutron Science Center), O'Brien dives into the intricate relationship between hydrogen and uranium behavior under stress.
- Mark Wartenbe's investigation into the largely hidden magnetic properties of plutonium. Employing the RLOUB and National High Magnetic Field Laboratory's Pulsed Field Facility at Los Alamos, Wartenbe's work aims to uncover thermodynamic signatures of magnetism in plutonium.
- Larissa Huston's crystallographic study of solid-solid phase transitions
 in uranium ditelluride, searching for signs of 5*f*-electron localization.
 Huston's research uses the diamond anvil pressure cell at the High-Pressure
 Collaborative Access Team beamline at Argonne National Laboratory's
 Advanced Photon Source.
- Stephanie Carpenter's work on *f*-block complexation with phosphide ligands aims to develop innovative separation techniques. Carpenter's project is a collaboration with teams from the University of New Mexico and the University of Rochester, utilizing the Radiochemistry Complex at Los Alamos.
- **Zach Jones's investigation** into the coordination chemistry of heavy actinides in aqueous environments, examining the effects of 5*f*-electron radial contraction. His work leverages advanced X-ray spectroscopy techniques at the Stanford Synchrotron Radiation Lightsource.

Through their research, these fellows are shaping the future of actinide science, ensuring its continued relevance and impact for generations to come.

Franz Freibert, Director G.T. Seaborg Institute for Transactinium Science

Improving Spectroscopic Understanding of Actinides

Joseph M. Kasper

One longstanding challenge in actinide science is understanding the reactivity and chemical bonding of actinide complexes. These complexes, such as those involving uranium, occur both naturally in the environment as well as artificially, as a component of nuclear waste. Ideally, one could separate out the various elements to both isolate hazardous material and reclaim and recycle valuable rare earth elements. This requires a thorough understanding of how strongly the different metals bind to other ions or molecules, known as ligands. Experiments with actinides are, however, challenging due to their radiological properties; fortunately, we can use theoretical models and perform calculations using quantum mechanics to better understand experimental data as well as explore both real and hypothetical complexes.

The main goal of computational chemistry is to solve the Schrödinger or Dirac equation for a system of electrons in the potential generated by the atoms in the molecule. Doing so allows one to predict any of its observable properties. However, due to the complexity of the many-body problem, these equations cannot be precisely solved in practice; instead, approximations must be made, requiring a careful balance of computational cost and accuracy. Understanding the accuracy of different levels of calculation is essential for advancing a predictive capability for actinide bonding that can be used to inform the most promising future chemistries. In this work, calculations using different levels of theoretical approximations and computational cost were performed to interpret experimental X-ray absorption spectroscopy (XAS) data on actinide bonding.

Measuring chemical bonds with X-rays

X-ray absorption spectroscopy is an experimental technique that has gained prominence as a method to analyze the bonding and electronic structure of metal complexes. In XAS, high-energy photons excite the tightly bound core electrons in atoms or molecules to unoccupied quantum mechanical states, as depicted in Fig. 1 (see p43 for an extended description of XAS). These levels are sensitive to bonding in the metal complex and its local environment such that small changes in the structure produce noticeably different spectra. With a theoretical framework or model, both the position and intensity of the peaks in the absorption spectrum can be interpreted and used to evaluate the strength and nature of chemical bonding.

One of the reasons XAS is very useful for studying bonding is the strong energy dependence on the atomic number of the element. This means that it is relatively easy to pick out a particular metal or ligand atom of interest and resolve specific spectral lines or peaks instead of having many overlapping features. While the idea of measuring metal bonding by probing the ligand atoms was initially used within transition metal (d-block) chemistry, scientists at Los Alamos have applied this technique to actinide complexes and were able to show that much richer chemistry occurs with the 5f elements than was previously understood. Unlike their lanthanide (4f) counterparts, in which the f electrons are well shielded from the valence electrons, in complexes with 5f elements, these electrons are exposed and able to participate in bonding. Depending on the particular ligands, oxidation



Joseph Kasper

Joseph Kasper is a Scientist at Los Alamos National Laboratory within the Materials and Physical Data group (XCP-5). Previously, he worked as a postdoc with Ping Yang and Enrique Batista in the Theoretical division at Los Alamos after he obtained his PhD in chemistry at the University of Washington under the supervision of Xiaosong Li. His research interests include the electronic structure of heavy elements, computational methods for excited states, and the prediction and understanding of spectroscopy.

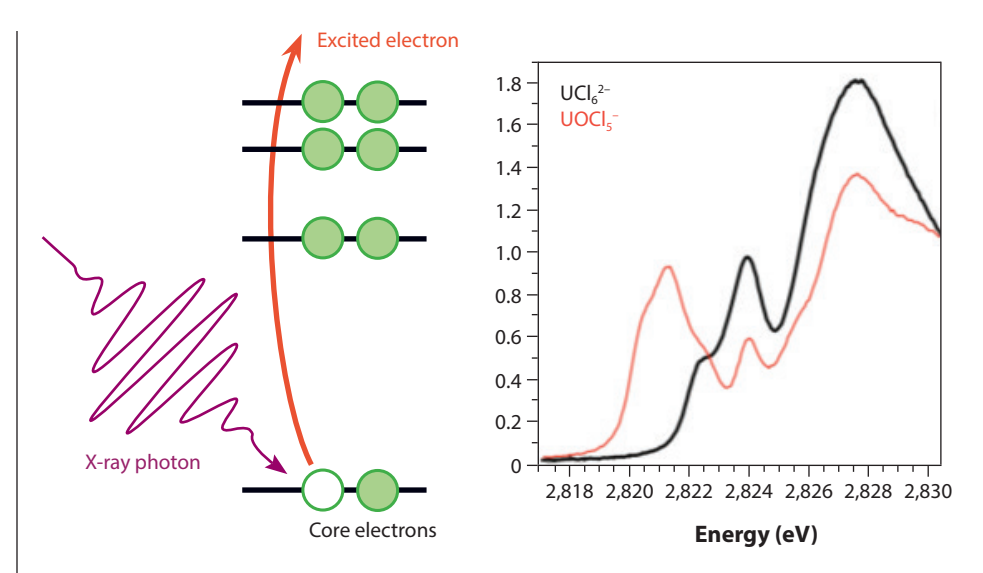


Figure 1. *Left*: Cartoon of an X-ray exciting an electron in a low energy "core" orbital to unoccupied levels. *Right*: Experimental XAS spectra of two different uranium complexes. While there is only one substitution of an oxygen (O) for a chloride (Cl), there are large changes to the electronic structure and resulting spectrum (courtesy of Minasian et al. in the Journal of American Chemical Society, 2012: see further reading for details).

• • •

state, symmetry, and energetic match, the amount of covalency can be tuned. The variations in chemical bonding available with actinide species have renewed interest in exploring the chemical space of actinide complexes for many different applications.

Advanced relativistic quantum chemistry calculations

For high-Z elements such as the actinides, ab initio calculations are complicated due to both a large number of electrons and the need to account for relativistic effects, because core electrons have large kinetic energies with effective speeds a significant fraction of the speed of light. To handle many electrons, the dominant method of choice is density functional theory (DFT). While DFT simplifies calculations by relying on a single density at each point in space rather than wavefunctions dependent on a large number of coordinates (3N, where N is the number of electrons), however, it requires an unknown functional. Nevertheless, good approximations to this unknown have been found by using theoretical constraints as well as fitting tunable parameters to experimental data.

Relativistic effects can be accounted for by solving the Dirac equation instead of the Schrödinger equation, at the cost of additional complex algebra. One of the most notable effects that can be seen spectroscopically is spin-orbit coupling, terms that account for a magnetic field generated by moving electrons that in turn influence a particle's quantum mechanical spin. As shown in Fig. 2, the radial distribution functions of valence orbitals in uranium are significantly affected by both scalar and spin-orbit corrections. This has strong implications for the strength of chemical bonding and interpretation of spectra.

As shown in Fig. 3, while calculations that ignore relativistic corrections work reasonably well even through the 5d block, there is a noticeable disagreement between calculations that include variational relativistic effects and those that do not for the uranium chloride complex. Note that while the changes to the radial distribution functions shown previously might appear small and hard to quantify,

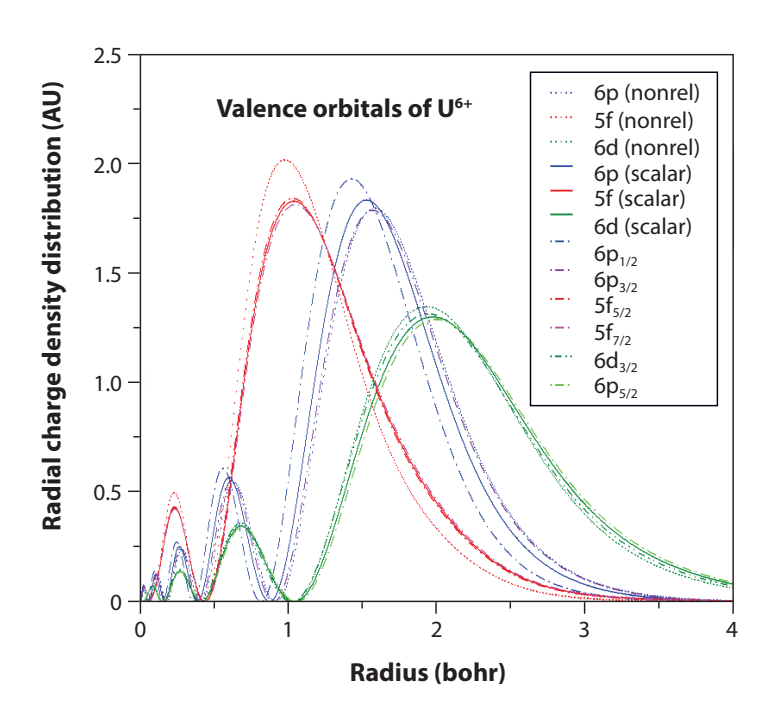


Figure 2. The calculated radial distribution functions for the valence orbitals of uranium show significant variations depending on how they are computed. The three levels of theory shown here are: (i) no relativistic corrections (nonrel), (ii) scalar relativistic corrections only, and (iii) scalar + spin-orbit.

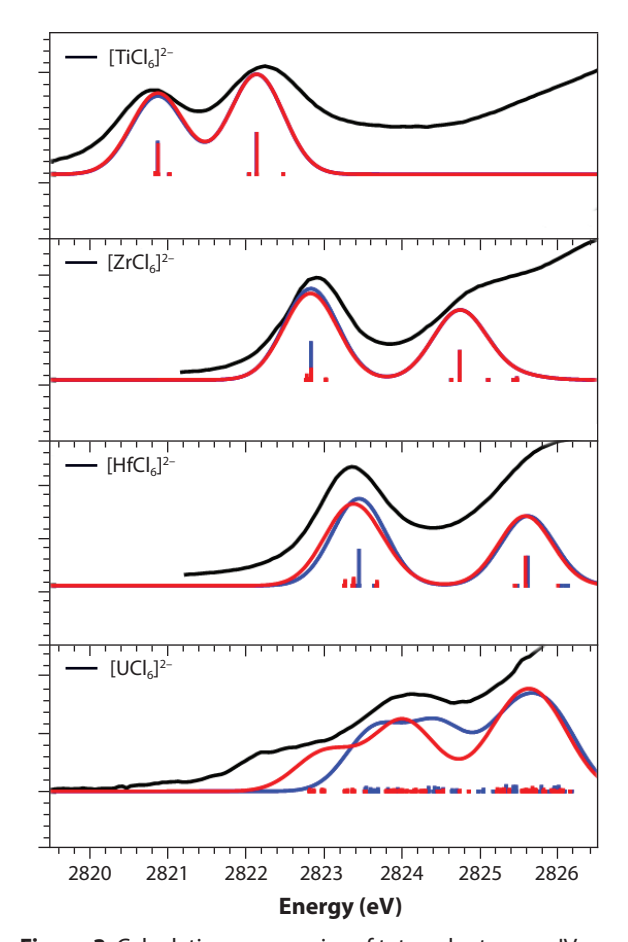


Figure 3. Calculations on a series of tetravalent group IV chloride dianions compared with the uranium analogue. Using the variational relativistic DFT treatment (red) show much better agreement with experimental X-ray absorption data (black) than the those without (blue).

predicting the spectra serves as a stringent test of the accuracy of a particular level of theoretical approximation due to the high sensitivity of X-ray spectra to the valence orbitals involved in chemical bonding.

Assessing the accuracy of approximations

Since variational relativistic calculations are significantly more expensive, there is a desire to use cheaper calculations when possible, either by ignoring certain terms or by using fitted potentials to simplify future calculations. Recently, we performed calculations of X-ray spectra of a variety of actinide complexes at several different levels of approximations and compared the accuracy with experimental data. Unsurprisingly, the more advanced calculations were more accurate. However, we were much more interested in the quantitative improvement. Specifically, we wanted to answer the question, "If we use this more complicated and expensive model, is it worth the effort?" Three models were compared and are shown schematically in Fig. 4. The most advanced method was known as X2CSO and included all electrons in a variational calculation with relativistic effects and spin-orbit coupling interactions. To test the value of these terms, we created a model in which these spin-orbit terms are ignored—the all-electron "scalar relativistic" calculation X2CSR model. The most inexpensive calculation was the relativistic effective core potential (RECP), a parametrized model to fit tightly bound core electrons that are not active in the problem.

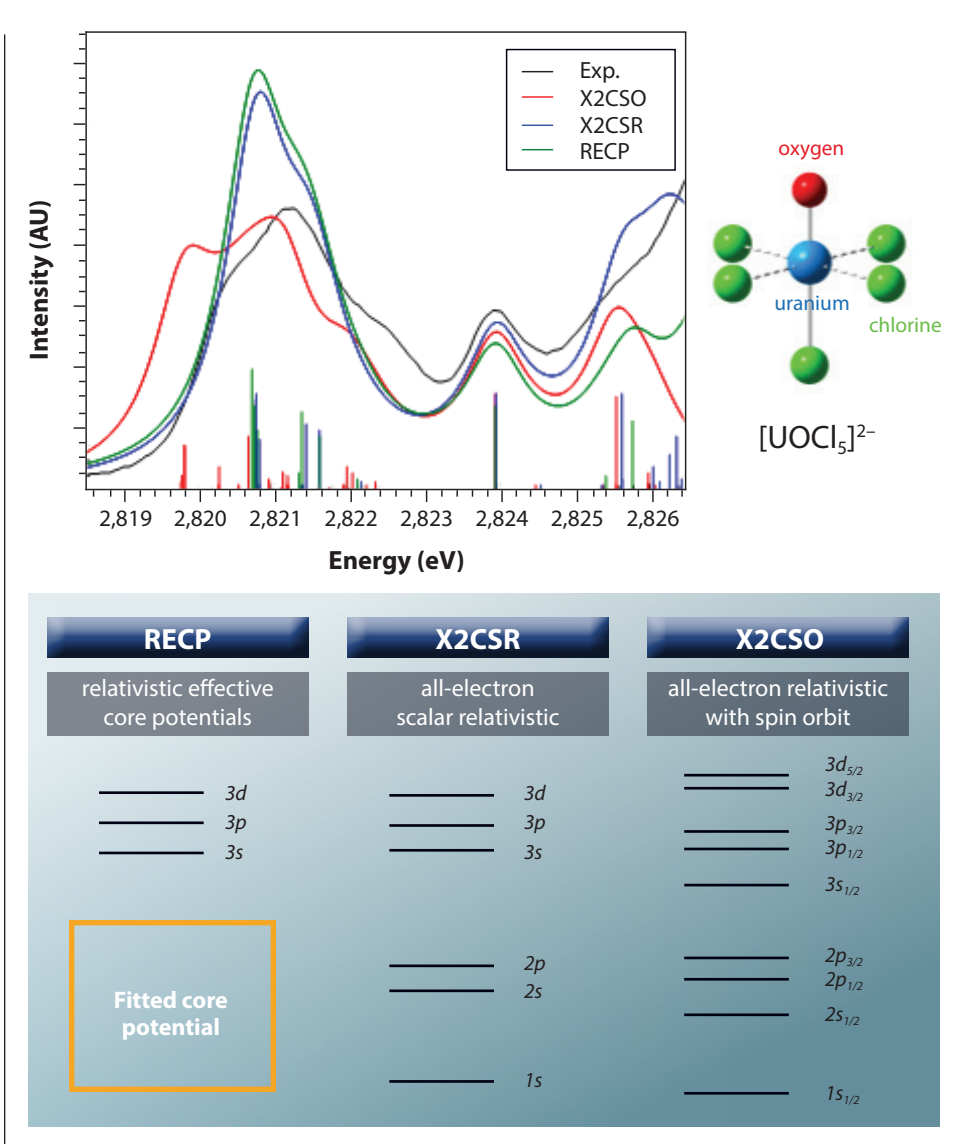


Figure 4. Spectra of [UOCl_s]²⁻ complex (*above*) computed with three different levels of theory (*below*) compared to experiment. From least to most accurate, left to right.

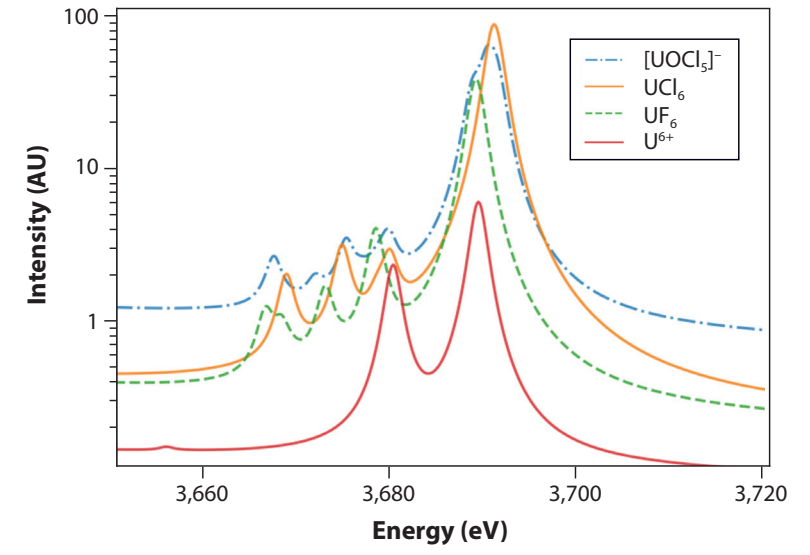


Figure 5. Calculated X-ray emission spectra are very sensitive to the chemical environment.

For the actinide complexes studied, it was very clear that including the spin-orbit interaction provided greatly increased accuracy. A typical reduction of error with experiment was around 25–30% lower than the scalar relativistic calculation. As shown in Fig. 4, there was also a significant change to the shape and number of features. On the other hand, using the RECP method only resulted in a loss of 1–2% in accuracy compared to the all-electron X2CSR. In other words, the much cheaper RECP model could make sense for a quick estimate, but there is little reason to use the all-electron relativistic calculation without the spin-orbit terms (X2CSR), as one would spend considerably more computational effort for nearly the same result.

Emission spectroscopy and future developments

While absorption spectroscopy has been extensively used, there has been renewed interest in using its partner, emission spectroscopy, and combinations of the two, also known as resonant inelastic X-ray scattering (RIXS). These methods provide complementary information, but can have significant advantages in improving experimental data such as reduced broadening of features. New computational tools for treating these spectroscopies are underway, as most computational chemistry methods are designed to treat the ground state and not the many highly-excited states required to model emission spectroscopy. As shown in Fig. 5, current methods can capture the qualitative features, though how quantitative remains an open question.

While the calculations discussed so far represent different approximations in the choice of which physics are incorporated in the Hamiltonian, there is still a significant loss of accuracy due to the approximation of DFT and incomplete treatment of electron correlation. New computational capabilities to use the configuration interaction and coupled-cluster many-body methods with the all-electron spin-orbit Hamiltonian are being developed within the community and are expected to be essential for quantitative accuracy on experimental techniques such as X-ray emission spectroscopy and RIXS. Due to exponential scaling with the number of orbitals included for correlation, much like mentioned before, one wants to know which additional computational cost is worth paying. Systematic study will not only provide benchmark calculations for DFT results, but also aid in our understanding of which sets of orbitals are most important to chemical bonding in actinides and shed light on longstanding questions about actinyl covalency.

Summary

As computational capability has increased, the ability to accurately calculate the spectroscopy of the actinides has also improved with new methodologies and levels of approximation. While one would wish to always use the most accurate calculation, it is important to balance computational cost. Systematic studies have revealed that the expected accuracy with increased computational cost is not linear; sometimes a large jump is seen, while it can also often be the case that a much more expensive model provides very little benefit. Understanding which approximations to use for a given problem at hand remains part of the art of computational work.

Acknowledgments

J.M.K. would like to acknowledge support from a postdoctoral fellowship with the Glenn T. Seaborg Institute and a Director's Postdoctoral Fellowship at Los Alamos National Laboratory, and the Department of Energy, Office of Science (DOE-OS), Basic Energy Sciences (BES) Heavy Element Chemistry Program (HEC) at LANL, as well as collaborators on this work: Ping Yang, Enrique R. Batista, Stosh A. Kozimor, and Xiaosong Li.

Further reading:

- S. G. Minasian et al. "Determining Relative f and d Orbital Contributions to M-Cl Covalency in MCl₆²⁻ (M = Ti, Zr, Hf, U) and UOCl₅⁻ Using Cl K-Edge X-ray Absorption Spectroscopy and Time-Dependent Density Functional Theory", J. Am. Chem. Soc., 2012, 134, 12, 5586.
- J. M. Kasper et al. "Relativistic Effects in Modeling the Ligand K-Edge X-ray Absorption Near-Edge Structure of Uranium Complexes", J. Chem. Theory Comput., 2022, 18, 4, 2171.



Mary O'Brien

Mary O'Brien was a Seaborg Institute Postdoctoral Fellow from April 2021 to April 2023 under the mentorship of Samantha Lawrence. She is currently a staff scientist on the Materials Compatibility team in the Sigma Manufacturing Sciences division at Los Alamos National Laboratory. Her research focus is understanding hydrogen embrittlement and corrosion phenomena in a wide variety of metallic systems using advanced characterization and mechanical testing methods, with a current focus on actinide materials.

Probing the Effect of Hydrogen on Uranium

Mary O'Brien

Hydrogen embrittlement is a long-standing challenge in metallurgy—early onset failures can occur in metallic systems after they are exposed to hydrogen, whether it is during manufacturing or while in service. For example, steel pipelines used to transport oil and gas are exposed to high hydrogen concentrations in the form of hydrogen sulfide gas, which has led to numerous instances of pipeline leaking or rupture. In uranium, even small amounts of hydrogen picked up during manufacturing processes like welding or salt-bath annealing are enough to cause an unexpected reduction in ductility. Reduced ductility early in manufacturing can result in unexpected cracking during downstream manufacturing processes like drawing. Furthermore, when metallic uranium is used in nuclear applications such as fuels, it can be exposed to hydrogenous environments (e.g., aqueous and acidic solutions), both in the reactor and during end-of-life storage. As one of the few institutions in the world entrusted with actinide research, Los Alamos National Laboratory has a duty to illuminate the failure mechanisms of uranium materials for both global security needs and nuclear power.

Hydrogen deformation mechanisms are elusive

The combination of strength and ductility required in many common engineering applications such as steel pipelines or cars is supplied largely from the high symmetry of the metallic crystal structures of such materials (Fig. 1a). Metals accommodate deformation largely by movement of defects, also known as slip, along a specific direction and plane, the combination of which is known as a slip system. Scientists and engineers have extensively studied the impact of hydrogen on these high-symmetry crystal structures, but despite a century of research, the mechanisms by which hydrogen causes early-onset failures are not well understood. This is partly because high-symmetry crystals have many symmetrically equivalent slip systems, which results in complex defect interactions that are difficult to decipher. Many engineering metals (nickel, aluminum, some stainless steels, etc.) have a face-centered cubic structure, containing two planes of atoms and six directions along which defects can move (Fig. 1a). The complex interactions that arise when defects interact along these planes and directions convolutes the interpretation of the effect of hydrogen on any individual mechanism.

Alpha-uranium, with its low-symmetry, orthorhombic crystal structure, provides a unique opportunity to assess hydrogen effects on deformation. Atoms in alpha-uranium are arranged in a corrugated structure (Fig. 1b), which has far fewer slip planes to accommodate deformation. As a result, alpha-uranium offers a unique opportunity to deconvolute the effect of hydrogen on deformation, providing insight into both uranium deformation and the broader mechanisms of hydrogen effects in metals.

Understanding hydrogen/uranium interactions is not without its own challenges. Hydrogen has an exceptionally low solubility in uranium at room temperature (~0.2 wppm). Upon saturation, it forms uranium hydride, which results in an approximate 70% volume expansion, posing significant safety problems as it is

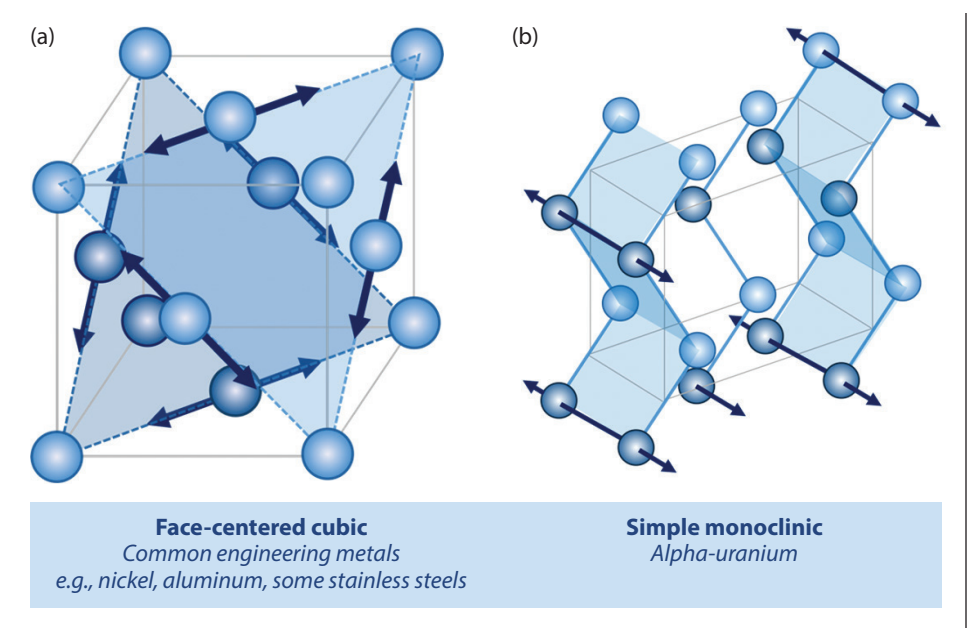


Figure 1. The crystal structures of (a) many common structural metals (e.g., aluminum, nickel) have higher symmetry than (b) alpha-uranium. Alpha-uranium contains far fewer slip planes to accommodate deformation (illustrated in blue with arrows), which potentially simplifies the deformation mechanisms, in particular for hydrogen embrittlement, allowing potentially for easier interpretation of the data and deeper insight.

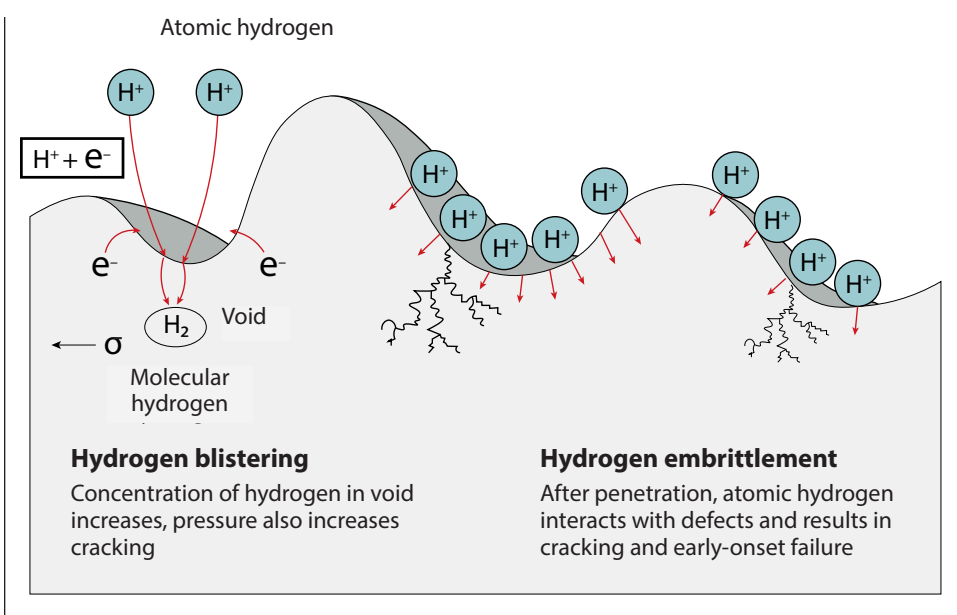
• •

pyrophoric (spontaneously combusts in oxygen). Due to the low solubility and high affinity for hydrogen, and accompanying safety issues, the study of hydrogen embrittlement in uranium has largely focused on understanding the initiation and growth of uranium hydride. However, many researchers have observed that the addition of hydrogen can still drastically reduce the ductility of uranium even at concentrations below the solubility limit.

Basic aspects of hydrogen embrittlement

Researchers have identified several different mechanisms to explain reductions in ductility from hydrogen, however, most relevant to our studies is the hydrogenenhanced localized plasticity (HELP) theory. This theory proposes that hydrogen affects defects, both in the way individual defects move and the larger structures that the accumulation of defects create. Plasticity results when a material permanently deforms—this permanent deformation starts with an internal defect movement, and accumulation of these defects can result in material failure. The defects relevant to this theory are line defects in the crystal, which are termed dislocations.

Supporting this theory, researchers have observed that hydrogen reduces the repulsive force between two defects, which results in higher defect densities in samples deformed in the presence of hydrogen. When too many defects accumulate locally, internal void or crack formation occurs. Thus, because more dense accumulations of defects occur in the presence of hydrogen than would occur in its absence, hydrogen can cause early onset failure. Historically, research has focused on studying these dense defect structures after fracture has occurred. However, more work is needed to understand the effect of hydrogen on initial defect movement before fracture occurs. This work explores the latter, examining the hypothesis that hydrogen reduces the amount of energy required to initiate movement of line defects.



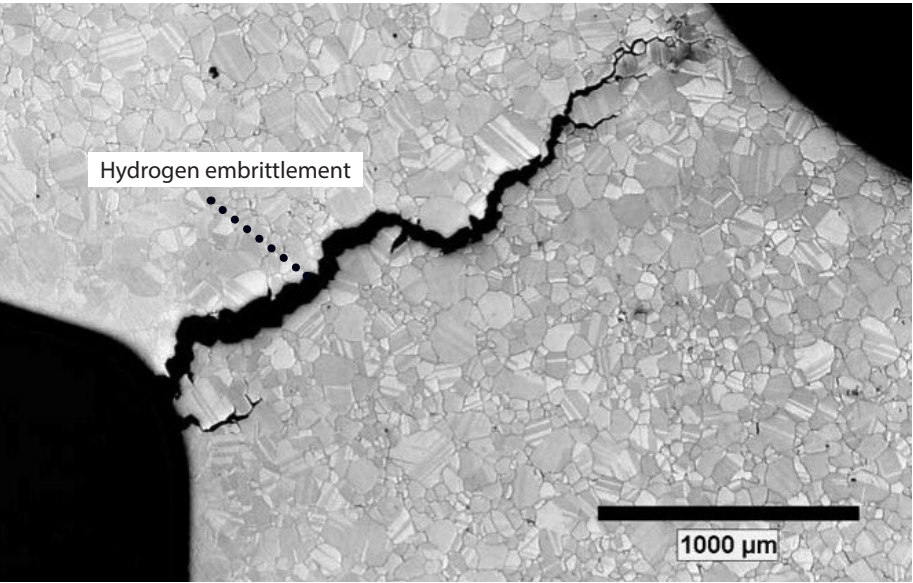


Figure 2. *Top*: Outline of the mechanisms of the effects of hydrogen on the surfaces of materials. *Bottom*: An example of hydrogen embrittlement in a nickel-based alloy showing signs of intergranular cleavage (courtesy of lannuzzi et al., "Materials and corrosion trends in offshore and subsea oil and gas production" in *npj Materials Degradation*, 2017).

• • •

The low-symmetry crystal structure of alpha-uranium poses both opportunities and challenges for observing the effect of hydrogen on initial defect movement. As described above, its low symmetry has fewer symmetrically equivalent slip systems, simplifying the deformation mechanism. However, its more complex macrostructure creates some difficulties. Within a larger piece of metal, there are groupings of similarly oriented crystals, referred to as grains. The distribution of orientations of these grains is known as crystallographic texture, which can be drastically affected by the manufacturing process. This is important for alpha-uranium because it results in deformation processes that are highly dependent on the orientation of the crystal, known as anisotropy.

Effects of processing on properties of uranium

Because of anisotropy in uranium, the traditional rolling process used with most metals (straight-rolling) has been modified by metallurgists to achieve more homogeneous properties (Fig. 3a). This more complicated process, called clockrolling, creates a much more homogeneous texture within the rolling plane. However, a different texture persists between the through-thickness direction and the rolling plane, which is seen in the electron backscatter diffraction (EBSD) inverse pole figure (IPF) micrographs for both of these directions (Fig. 3b).

A result of the differences between the rolling plane and through-thickness textures is that deformation is accommodated by different mechanisms depending on how a testing specimen is machined from a plate. In a through-thickness sample (Fig. 3a), the stress is largely accommodated by movement of line defects (i.e., dislocations). In contrast, in the rolling plane direction, stress is accommodated by a mechanism called twinning (details of which can be found elsewhere but are not the focus of the current work). Because we seek to understand the effect of hydrogen on the onset of line defect movement, discussion of results will be limited to the through-thickness textured specimens.

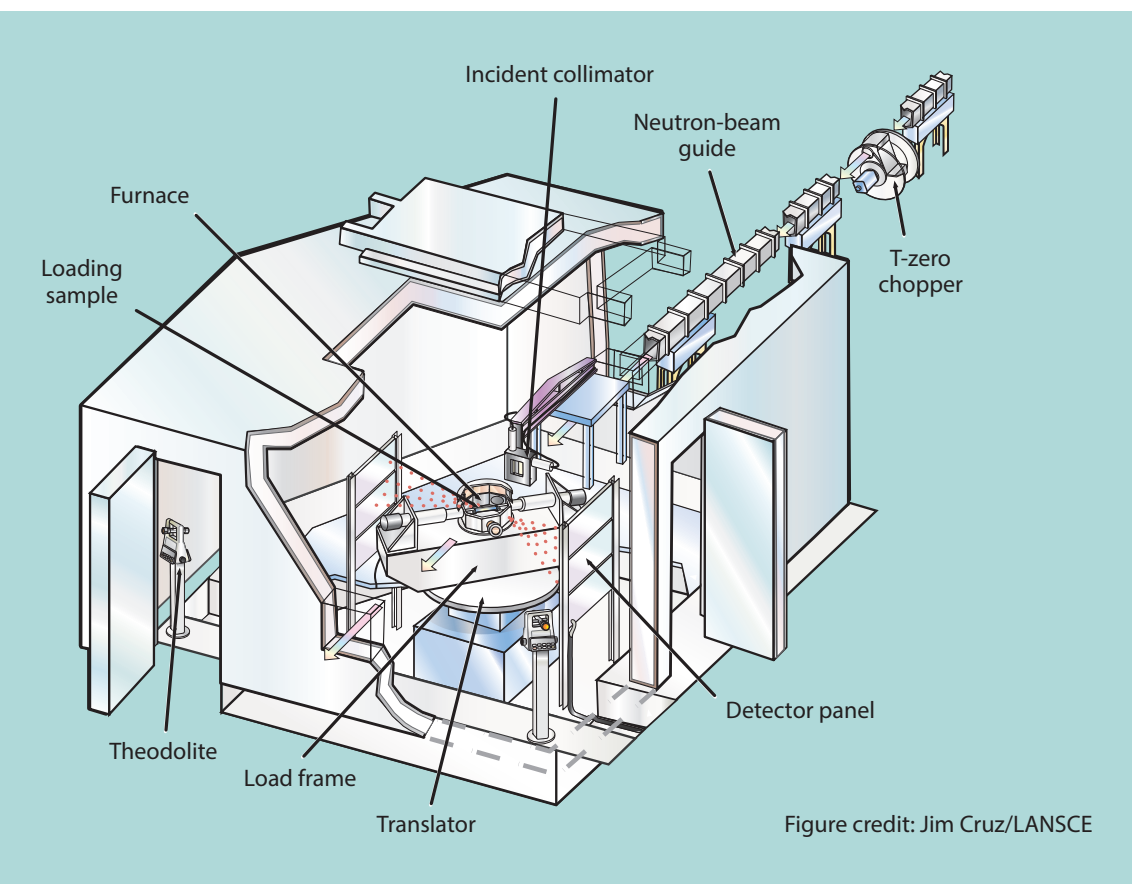
Hydrogen charging and in situ elastic lattice strain measurements

Our hypothesis is that hydrogen lowers the energy necessary for the initiation of line defect movement, thus causing early onset plasticity. To test this, in situ neutron diffraction data were obtained during compression tests using through-thickness textured clock-rolled depleted uranium. Although hydrogen embrittlement tests are typically conducted using tension and discussed in terms of reductions in ductility, the initiation of defect movement is a phenomenon that occurs regardless of the direction of externally applied stress. Because compression specimens are simple cylinders compared to the more complex geometries required for tension specimens, compression was chosen for this initial study. To circumvent the low solubility of hydrogen in uranium at room temperature, hydrogen was introduced during heat treatment at an elevated temperature and "quenched" into place using a well-established hydrogen-charging process. To achieve this process, samples were placed in a quartz tube sealed at one end and attached to a vacuum-gas manifold at the other end (Fig. 4). All samples were first exposed to vacuum at 630 °C for two hours to remove any hydrogen from manufacturing processes. Hydrogen-charged samples were then exposed to a known volume and pressure of a gas mixture containing 99% argon and 1% hydrogen at 630 °C for one hour, while uncharged samples remained in vacuum under identical conditions (without hydrogen). Both the hydrogen-charged and uncharged experiments were concluded by breaking the quartz tube in water. This "quenching" step reduces the energy and reaction time available for uranium hydride formation.

Neutron analysis at LANSCE

Once heat treatment with and without hydrogen was performed, samples were sent to the Los Alamos Neutron Science Center (LANSCE). The texture of the specimens was first measured using the High-Pressure-Preferred Orientation (HIPPO) diffractometer, then sent to the Spectrometer for Materials Research at Temperature and Stress (SMARTS; see sidebar). Using SMARTS, the samples were compressed, and neutron diffraction data was collected in situ. For these experiments, if defect movement initiated on a particular set of planes, a transition to plastic strain would be observed. It was hypothesized that this transition to plastic strain, indicative of the initial movement of defects, would occur at lower stresses in hydrogen-charged specimens.





SMARTS at LANSCE

The Spectrometer for Materials Research at Temperature and Stress (SMARTS) is a neutron diffractometer optimized for the study of engineering materials. It is one of several instruments available at the Lujan Center, which has the capacity for 16 beamlines (not all being used concurrently) and is one of five user facilities supported by the Los Alamos Neutron Science Center (LANSCE) accelerator. SMARTS is a specialized instrument that allows the measurement of deformation under stress and extreme temperature, and the measurement of spatially-resolved strain fields.

The instrument is particularly useful for making measurements under conditions similar to the processing or operating conditions for the material. This is relevant for determining stress in fabricated components, in situ loading in new materials, and for process monitoring, and has been used to solve problems ranging from certifying fuel plates for nuclear reactors and identifying failure mechanisms in turbine blades to predicting the lifetime of bridges. SMARTS was originally built (in 2001) to work with a wide range of materials, measuring from 1 mm³ to 1 m³ and weighing up to 1,500 kg, under extreme loads (250 kN) and temperatures (1,500 °C). It can also handle radioactive materials and classified experiments.

Bjørn Clausen, the scientist in charge of SMARTS operations, says that the instrument was the first timeof-flight neutron diffractometer built specifically for engineering-relevant measurements. "Before this," he explains, "these measurements were performed using converted general-purpose diffractometers, which had significant space constraints that limited the sample size and use of ancillary equipment such as load frames." He adds that, "We have had a large friction stir welder in SMARTS two meters on the side, if not more, weighing nearly one ton. That could not happen in the older instruments. This enabled measurements of internal stress and microstructure variations in the stirring tool, and as a function of distance away from the tool." Several similar instruments have been built since, leveraging the success and design of SMARTS, including EnginX at the ISIS Neutron and Muon Source (in the UK), VULCAN at the Spallation Neutron Source at Oak Ridge National Laboratory, and Takumi at JPARC (Japan Proton Accelerator Research Complex). Clausen says, "I wouldn't directly call them copycats, as there are improvements and optimizations for each of them."

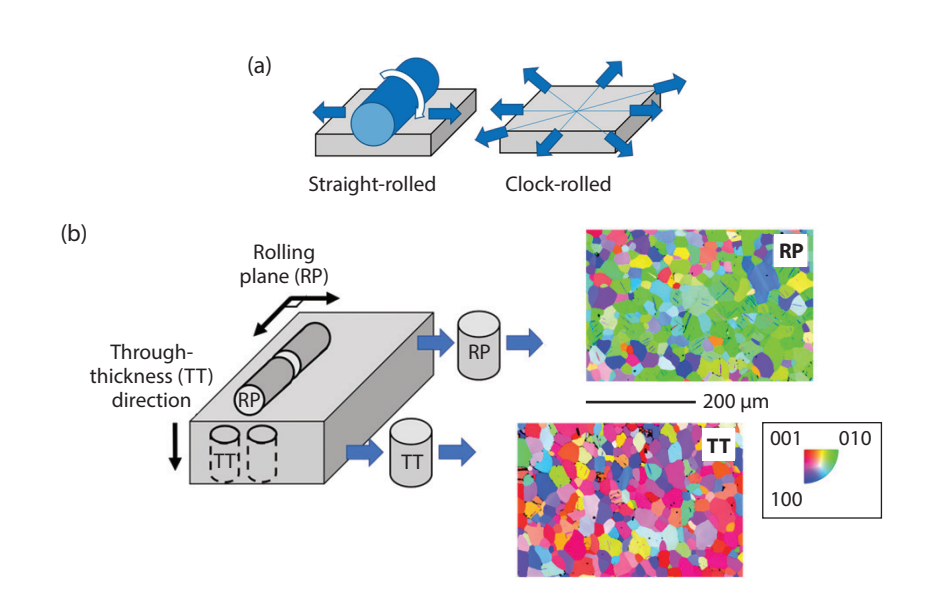


Figure 3. (a) Schematics representing the difference between traditional straight-rolling (left) and clock-rolling (right). (b) Schematic denoting the orientations of specimens machined from the rolled plate with accompanying electron backscatter diffraction (EBSD) inverse pole figure (IPF) micrographs demonstrating differences in texture. Colors represent grain orientation according to the inset colored stereographic triangle. [RP = rolling plane; TT = through-thickness direction]

"Uranium affords a unique opportunity to study the effect of hydrogen on the deformation of metals"

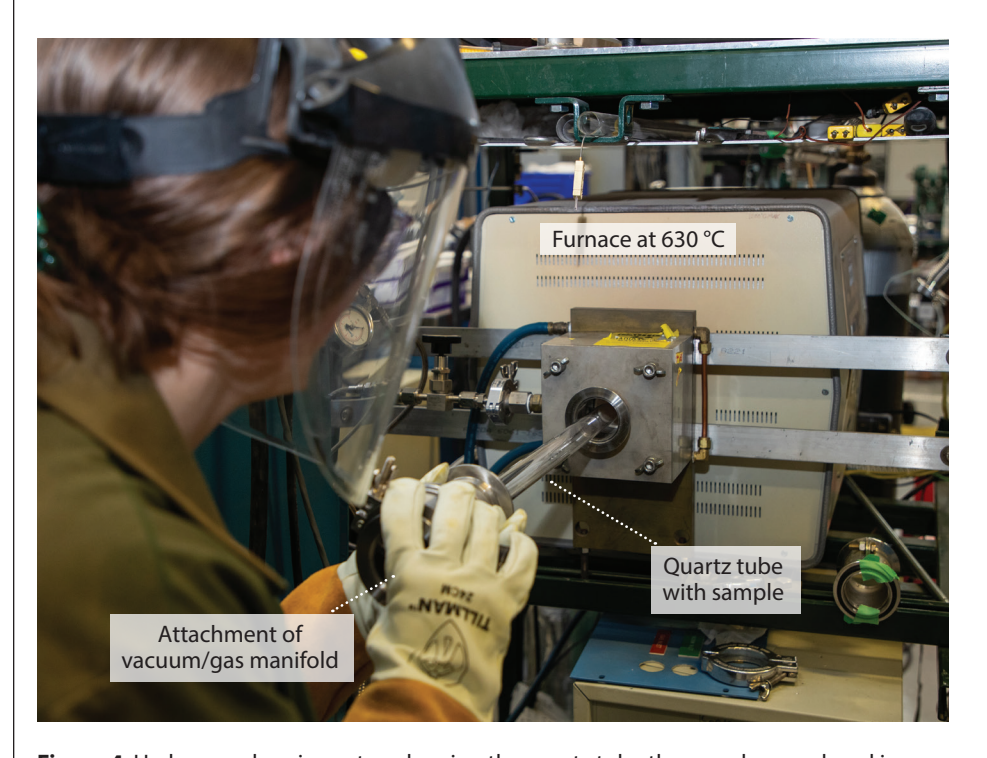


Figure 4. Hydrogen-charging setup showing the quartz tube the sample was placed in, attachment of the vacuum/gas manifold, and the tube furnace.

True stress-strain curves from the in situ experiments are shown in Fig. 5. The hydrogen-charged sample was only exposed to 3% strain, rather than the 5% strain the uncharged sample was subjected to, due to time constraints on the beamline. Although the hydrogen-charged sample exhibited slightly higher stresses for a given strain than the uncharged samples, the differences are not large enough to be considered significant.

Effect of hydrogen on stress relaxation of alpha-uranium

The initial theory guiding this work was that hydrogen would cause early onset plasticity, or divergence from elastic behavior, due to a reduction in lattice friction it induced. Therefore, in addition to the macroscopic stress-strain behavior in Fig. 5, elastic lattice-strain data was collected at every "serration" visible in the curve (indicated by a gray dashed box in Fig. 5). During the in situ experiments, the crosshead of the mechanical testing frame was paused for around 15 minutes, when neutron diffraction measurements were obtained. During this pause, the sample was held at a constant displacement, but exhibits a relaxation, or reduction, in stress. Once a diffraction dataset was obtained, the sample was then loaded again until the next pause—this stress relaxation followed by re-loading appears as serrations in the stress-strain data in Fig. 5. Unfortunately, the lack of significant difference between the elastic lattice-strain evolutions of the hydrogen-charged and uncharged samples means our hypothesis could not be proved by this experiment.

Typically, stress data obtained during diffraction holds is ignored as it is not the primary focus of the in situ experiments. However, valuable information about the motion of defects can be gleaned during stress relaxation. Rather than graphing stress as a function of strain, the same stress data shown in the gray box in Fig. 5 can be graphed as a function of time during the pause for diffraction collection, showing that stress decreases exponentially until reaching an asymptote (Fig. 6).

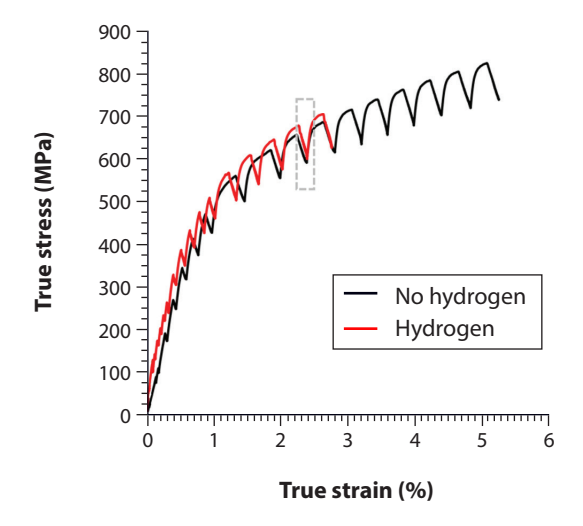


Figure 5. True stress-strain data from in-situ experiments using the SMARTS neutron diffractometer, demonstrating no significant difference in samples compression tested with (red) and without (black) hydrogen pre-charging, with an example of "serration" indicative of stress relaxation outlined in a grey dashed box.

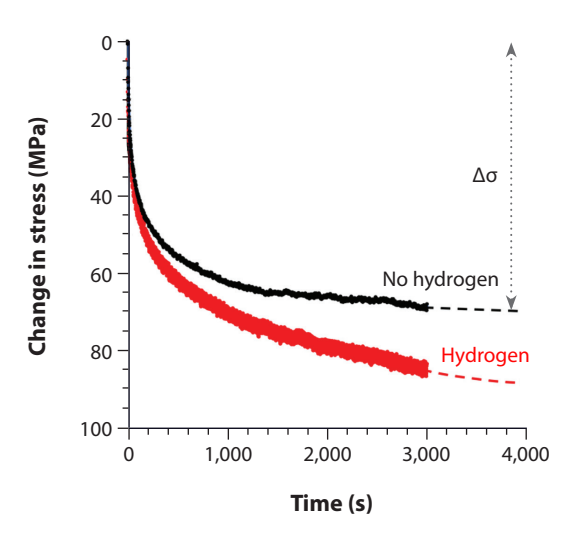
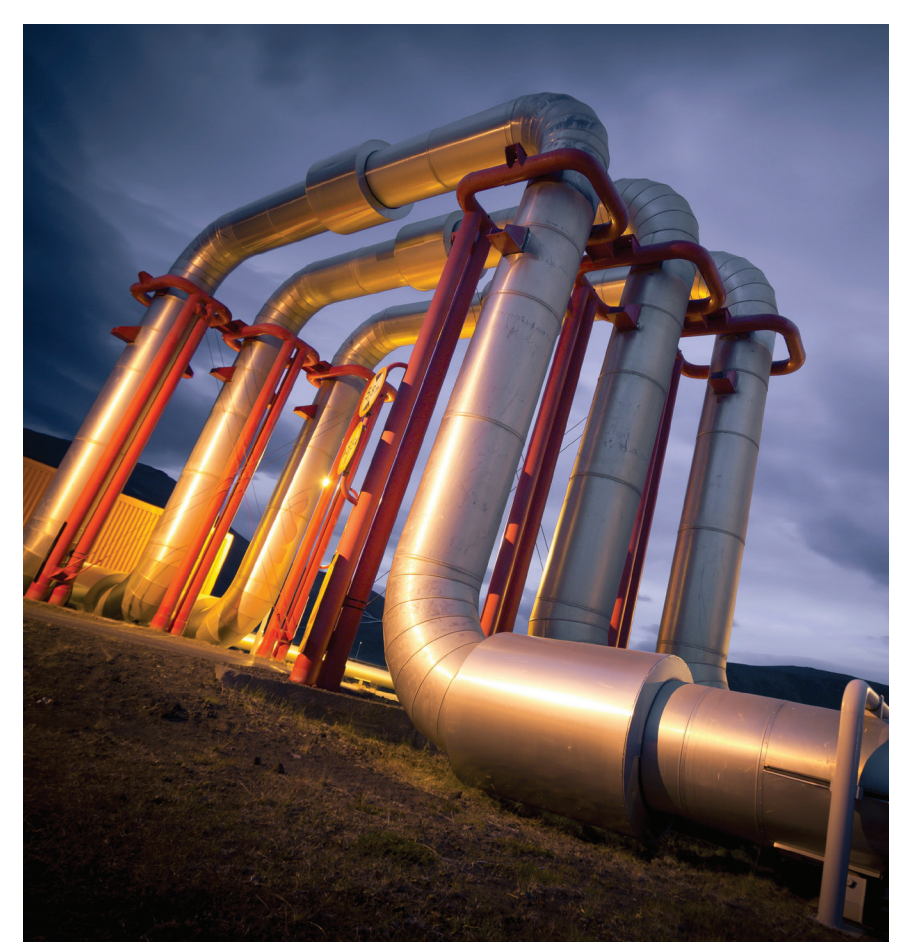


Figure 6. Example of stress relaxation curves obtained during diffraction holds at 2.6% strain (gray box in Fig. 4) in the hydrogen-charged (red) and uncharged (black) conditions. This data shows that hydrogen-charged samples exhibit a larger change in stress during the hold than uncharged samples.

Actinide Research Quarterly -





Steel pipelines used to transport oil and gas are exposed to high hydrogen concentrations in the form of hydrogen sulfide gas, which has led to numerous instances of pipeline leaking or rupture through hydrogen embrittlement. In uranium, even small amounts of hydrogen picked up during manufacturing processes like welding is enough to cause an unexpected reduction in ductility.

Preliminary analysis of the stress-relaxation behavior during each of the "serrations" indicates that hydrogen-charged samples exhibit a larger change in stress during the hold than uncharged samples. A greater change in stress reflects a greater mobility of defects and, therefore, shows that hydrogen charging has resulted in a greater mobility of defects in this manufacturing condition of alpha-uranium. This enhanced stress relaxation due to hydrogen has been observed in more common engineering materials with high-symmetry crystal structures such as steels. However, to the author's knowledge, this is the first observation of hydrogen impacting stress relaxation, and therefore defect mobility, in alpha-uranium. This enhanced mobility of defects due to hydrogen could be due to a change in the structure of defects or an effect on the barriers to defect motion. Future work could investigate these mechanisms by coupling advanced in situ microscopy techniques with molecular dynamics models of defects with and without hydrogen. Other work could also examine the effect of longer hydrogen exposures on strain-rate sensitivity.

Summary

Uranium affords a unique opportunity to study the effect of hydrogen on the deformation of metals due to the reduced number of deformation mechanisms available in its low-symmetry structure in the alpha phase. This work set out to understand the effect of hydrogen on the onset of defect movement, also known as the transition from elastic to plastic behavior. This hypothesis was initially tested by measuring in situ lattice strains on families of planes during compression at the SMARTS neutron beamline at LANSCE. Unfortunately, this in situ elastic latticestrain data did not provide any direct evidence that hydrogen affects the initiation of defect movement on individual lattice planes. However, by using stress-relaxation data that is typically ignored, it was observed that hydrogen significantly increased stress relaxation during pauses in displacement. This enhanced relaxation indicates increased defect mobility due to hydrogen. To the author's knowledge, this is the first observation of the impact of hydrogen on the stress-relaxation behavior of alphauranium. Understanding the effect of hydrogen on deformation in a low-symmetry crystal structure will not only provide crucial insights into the effect of hydrogen on deformation mechanisms in uranium but will also provide a fresh perspective on the influence of hydrogen on metallic systems more broadly.

Acknowledgments

This work is a collaborative effort with several other researchers: Samantha Lawrence, Jason Cooley, Allie Glover, Bjørn Clausen, Donald Brown, Robin Pacheco, Dan Savage, and Sven Vogel all contributed to and played vital roles in this ongoing project. Financial support was provided by the U.S. Department of Energy through the LANL/LDRD program and the Seaborg Institute for the postdoctoral fellowship to Dr. O'Brien. The editor (OTS) would like to thank Sam Burleigh, Bjørn Clausen, Michael Mocko, and Jim Cruz for their assistance in writing the SMARTS sidebar.

Further reading:

- 1. K.O. Findley, S.K. Lawrence, M.K. O'Brien, "Engineering challenges associated with hydrogen embrittlement in steels," in Encyclopedia of Materials: Metals and Alloys, Elsevier, 2022, pp. 235–249.
- 2. P.J. Ferreira, I.M. Robertson, H.K. Birnbaum, "Hydrogen effects on the interaction between dislocations," Acta Mater., 1998, 46, 5, 1749.
- 3. H.K. Birnbaum, P. Sofronis, "Hydrogen-enhanced localized plasticity—a mechanism for hydrogen-related fracture," Mater. Sci. Eng. A, 1994, 176, 1–2, 191.
- 4. M.L. Martin, M. Dadfarnia, A. Nagao, S. Wang, P. Sofronis, "Enumeration of the hydrogen-enhanced localized plasticity mechanism for hydrogen embrittlement in structural materials," Acta Mater., 2019, 165, 734.
- 5. C.S. Barrett, M.H. Mueller, R.L. Hitterman, "Crystal structure variations in alpha uranium at low temperatures," Phys. Rev., 1963, 129, 2, 625.
- 6. J.S. Morrell, M.J. Jackson, Eds., Uranium Processing and Properties. New York, NY: Springer New York, 2013.
- 7. R.J. McCabe, L. Capolungo, P.E. Marshall, C.M. Cady, C.N. Tomé, "Deformation of wrought uranium: Experiments and modeling," Acta Mater., 2010, 58, 16, 5447.
- 8. D.W. Brown et al., "Temperature and direction dependence of internal strain and texture evolution during deformation of uranium," Mater. Sci. Eng. A, 2009, 512, 1–2, 67.
- 9. C.A. Calhoun, E. Garlea, T. Sisneros, S.R. Agnew, "Effects of hydrogen on the mechanical response of α-uranium," J. Nucl. Mater., 2015, 465, 737.



Mark Wartenbe

Mark received his PhD in 2018 for his work on actinide-based superconductors at the National High Magnetic Field Laboratory Pulsed Field Facility at both Los Alamos National Laboratory and Florida State University. He continued his pulsed-field measurements at Los Alamos, focusing on actinides and plutonium in particular.

Magnetostriction Studies of Alpha Plutonium

Mark Wartenbe

Plutonium is a fascinating material which hosts a range of unusual behaviors. It has an unprecedented number of solid phases, significant volume changes between some of these phases (Fig. 1), negative coefficients of thermal expansion, and a very unusual 5*f* electronic structure, which is highly debated among theorists. This electronic structure is thought to be central to plutonium's myriad phenomena. For example, although plutonium would be expected to have a magnetically ordered, antiferromagnetic ground state, to date, no experimental evidence has been found for static magnetism from localized magnetic moments (ordered or disordered) in either the undefected alpha- or delta-phases (arguably plutonium's two most important phases). This mystery continues to challenge *f*-element theory and demands more sophisticated experimental approaches for investigation.

The uniqueness of plutonium is driven almost entirely by the character of its valence 5f electrons, which fall between the spatial limits of being either well localized or fully itinerant. The only other element that approaches this complexity is cerium, the first lanthanide element with an f-electron configuration (4f¹). Again, it is the f electrons that are responsible for the similarities in the two elements' chemical and physical properties (with cerium showing four allotropes). Along with these phenomena is the question of magnetism in these materials, or rather the lack of. Localized electrons tend to produce a magnetic moment and a larger lattice, whereas itinerant electrons produce a tightly bound lattice and metallic behavior. This can be clearly seen in the size of atomic lattices across the actinide series. Actinide elements lighter than plutonium exhibit smaller lattices and metallic behavior with increasing atomic number, while elements heavier than plutonium exhibit more localized electronic behavior and larger lattices (see Larissa Huston's article Actinides Under Extreme Pressures on p20 for a more detailed description of this phenomenon). Plutonium sits right in the middle of this changing behavior, and indeed its change in volume from the alpha- to delta-phase fills this discontinuity quite well. Although every study to date has failed to find any magnetic ordering in plutonium, this does not mean that electron spin or localized magnetic moments are not important.

In this study, we used the parameters of low temperature and high magnetic fields to explore magnetostriction in alpha plutonium, that is, how the physical size of the material changes with an applied magnetic field. This effect is most recognizable as the source of "humming" from the magnetic field-induced dilatometric response of an electrical transformer's ferromagnetic core—the alternating current, positive to negative, causes corresponding changes in alternating magnetic strain on the iron. To achieve these small-scale dimensional measurements in a non-ferromagnetic material, we used capacitive dilatometry, which offers high-resolution measurements and small instrument size that proved vital in these experiments. The results show an intriguing crossover between low temperature electron coherence and higher temperature behavior.

Kondo effect

Central to the discussion of plutonium physics is the concept of the Kondo effect. Jun Kondō proposed a model in 1964 describing the upturn in resistivity seen in nonmagnetic metals with dilute magnetic impurities at very low temperatures. This concept has been extended in the Kondo lattice model, in which the localized magnetic moments of the lattice ("magnetic impurities") are "quenched" by spin antiparallel coupling with electrons from the conduction band. Kondo lattice behavior often manifests as an electrical resistance that rises with lowering temperature, reaching a peak then sharply dropping as scattering from localized moments is reduced by the coupling of the fixed lattice moments and conduction electrons spins. This effect is seen in numerous compounds and alloy systems. Although alpha-manganese and curium exhibit a similar electrical resistivity response from antiferromagnetic ordering, plutonium appears to be the only non-antiferromagnetic element that displays this behavior.

Low temps, high fields, and tiny dimensional changes

To probe the unusual electronic behavior of plutonium, we applied low temperatures (1.3–300 K) and high magnetic fields (up to 15 T) to an alpha plutonium sample and measured the resulting dimensional changes. Low temperature studies allowed investigation of energy scales and phenomena that are normally hidden by higher temperature effects. Note that in this temperature range, plutonium exclusively adopts the alpha phase, which is stable up to 385 K. Magnetic fields are commonly used in condensed matter physics to probe low temperature behavior—in our context,



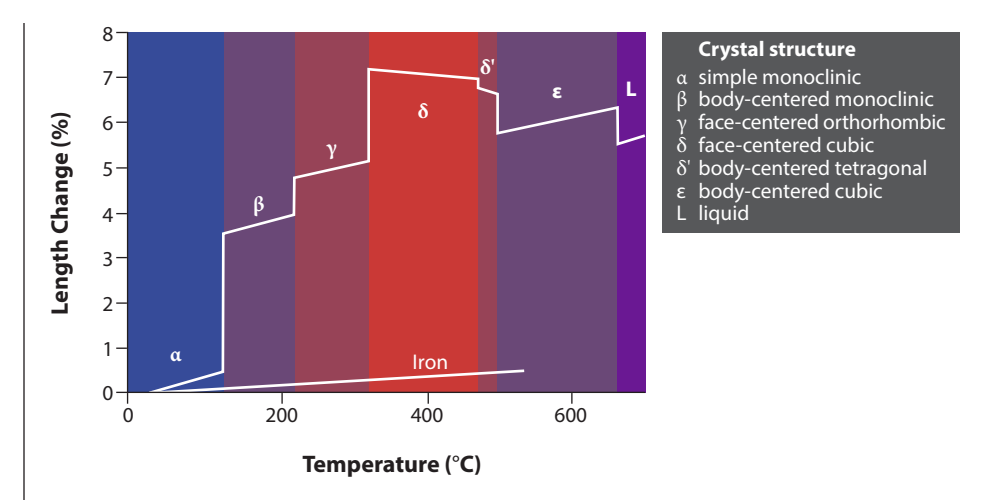


Figure 1. The remarkable effect of temperature on elemental plutonium, which displays multiple allotropes and significant volume changes; iron shown as an example of typical metal behavior.

• • •

magnetic fields are unique because they couple to magnetic moments very effectively while only weakly affecting the underlying lattice. This allows direct examination of plutonium's electronic structure while leaving the bulk of the sample unperturbed, unlike many other techniques. Very large magnetic fields are needed to observe even small volume changes with magnetostriction, and the resulting changes in the material therefore also require very precise measuring devices. Dimensional changes can be precisely measured as a function of temperature using dilatometers, and capacitive dilatometers, in particular, are uniquely suited for low temperature studies, with their small size allowing them to be fully inserted into many commercially made cryogenic systems (Fig. 2).

Improved dilatometry methods and a hidden order in delta plutonium

Previous dilatometry and magnetostriction work has focused on various delta plutonium materials using an optical fiber Bragg diffraction method. This method successfully found a crossover in gallium-stabilized delta plutonium from a positive magnetostriction response to a negative one (i.e., changing from expansion to contraction), revealing a previously hidden, yet substantial, contribution to the electronic structure of delta plutonium under an applied magnetic field. While fiber Bragg optical dilatometry offers many advantages, it has a relatively low sensitivity (10⁻⁸ m) and requires gluing a sample to the fiber in question. Thermal cycling is particularly stressful for these techniques, as the samples tend to become unglued with constant thermal contraction and expansion. Capacitive dilatometry, however, relies on a dilatometer containing two parallel capacitor plates and remains fixed over an unlimited number of thermal cycles. Samples are mounted in contact with one of the capacitor plates which is allowed to move freely against a spring, while the other plate remains fixed—thus, as the sample changes size, the plate distance also moves. These devices require a long process of assembly, thermal exercising, and background characterizations. However, the benefit is an unmatched resolution of 10⁻¹² m, firmly in the sub-angstrom range. This is the first time that this technique has been applied to plutonium, and it offers an improvement in both sensitivity and versatility compared to the more widely employed push-rod dilatometry technique.

Samples of plutonium cut into $2\times2\times2$ mm cubes were loaded into dilatometers that were then placed into custom-made brass containment cans. A sintered, stainless steel frit was fixed to each can as a HEPA filter , allowing gas exchange and ensuring thermalization while eliminating the possibility of system contamination. This setup was attached to a custom-made probe and lowered into a magnet variable temperature insert (VTI) system capable of a temperature range of approximately 1.3--300~K. After stabilizing the temperature, the magnetic field was swept at a low rate to prevent inductive heating from 0 to 15 T.

Magnetostriction data: Comparing alpha and delta plutonium

We were able to easily resolve the signals, which consisted of a largely quadratic and relatively flat signal response due to their small magnitude; magnetostriction response versus temperature is plotted in Fig. 3 (note that the magnetostriction coefficient is the fractional change in volume). The value of dimensional change for alpha plutonium is very small, which is expected for such a non-magnetic material—a similarly sized signal was also seen in previous gallium-stabilized delta plutonium work, again attesting to the small magnetic response of plutonium. However, while the coefficient changes sign from positive to negative in the case of gallium-stabilized delta plutonium, there is no change for undoped alpha plutonium. Instead, we see an increasing magnetostriction coefficient (i.e., expanding sample

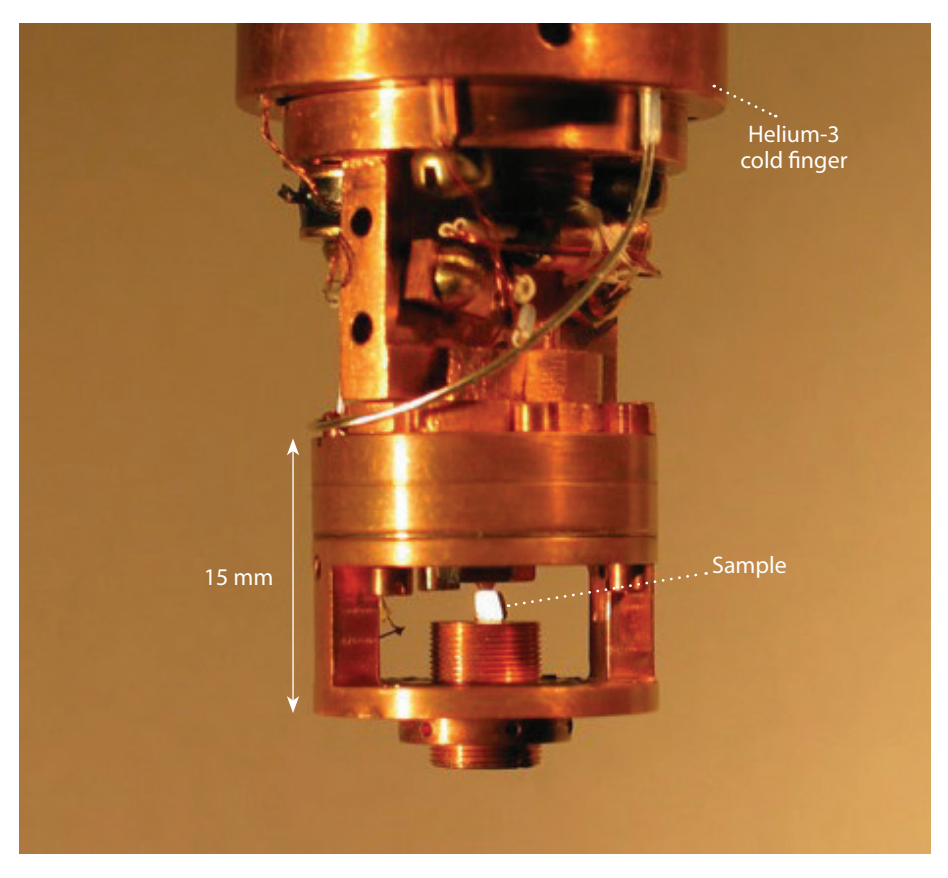


Figure 2. A capacitive dilatometer measures a change in sample dimension by detecting the capacitance between two parallel plates. One of these plates is fixed and the other is allowed to move as the sample changes size. The small size of the instrument makes it ideally suited for low temperature studies.

size) with increasing temperature from around 100 K upward, in the 10^{-8} m range. Below 100 K, there is a discontinuous break in the coefficient trend, with the low temperature coefficients being much larger and more constant over the temperature range (0–70 K). This characteristic change corresponds roughly in temperature with the theorized onset of Kondo coherence, which can be seen in literature values of resistance.

Above the proposed Kondo coherence temperature (50–100 K), we analyzed the magnetostriction response in a similar manner to our previous approach using gallium-stabilized delta plutonium. Prior data gave strong evidence for a higher energy state that is both smaller in volume and higher in magnetic moment. Both characteristics point to a stabilization of the beta phase, which not only has a smaller volume than the delta-phase but also has the largest magnetic moment of all plutonium phases. Likewise, we see a similar phenomenon in the higher temperature data obtained for alpha-phase plutonium. Field-tuned states among the heavy elements are not unprecedented; for example, certain cerium alloys change from the low temperature alpha-phase to the room temperature gamma-phase with the application of a magnetic field.

Meanwhile, the low temperature data (< 75 K) show a relatively high quadratic coefficient value and a much flatter temperature dependence. To gain further insight, resistivity for alpha-phase plutonium (literature data) was plotted alongside the magnetostriction data (Fig. 3). The peak in resistance at 75–100 K marks the

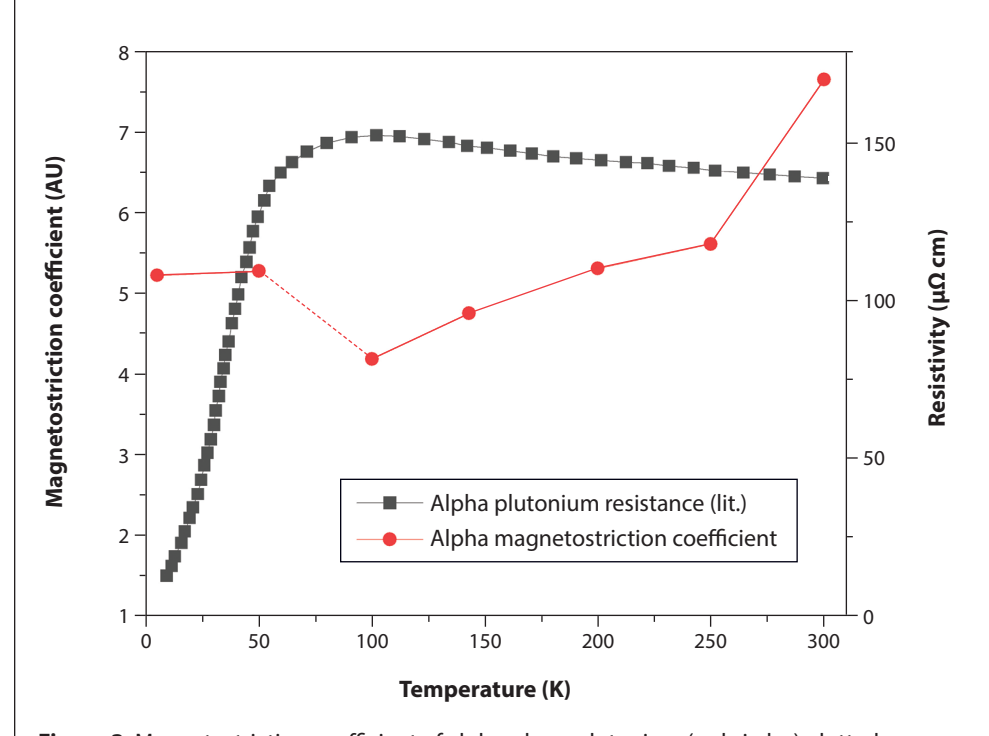


Figure 3. Magnetostriction coefficient of alpha-phase plutonium (red circles) plotted alongside literature data for resistivity (gray squares). The onset of Kondo coherence is seen as a peak in resistance between 50 and 100 K, which is reflected by a drop in magnetostriction in this range (dotted line). Increasing values of magnetostriction at higher temperatures indicate the appearance of a magnetic phase, possibly the beta phase.

theorized onset of Kondo coherence in the material, when conduction electrons begin to screen the lattice moments, thus reducing electron-lattice scattering and resistance. The discontinuous jump in behavior occurs exactly in this transitional region. Limited points on the low-end data (< $100~\rm K$) make analysis difficult, but it is clear that two distinct regions of different behavior correspond to the potential onset of Kondo coherence in alpha plutonium.

Summary

The complexity of plutonium's electronic structure creates unique structural and magnetic effects, including non-magnetic phases, unprecedented among the elements and still poorly understood. We used low temperatures (1.5-300 K) and high magnetic fields (up to 15 T) to explore the magnetostriction of plutonium, i.e., how the material physically expands or contracts under an applied magnetic field. Previous work explored the gallium-stabilized delta phase using an optical fiber Bragg diffraction method; in our work, we chose to examine undoped plutonium—alpha phase in the temperatures explored—using a more sensitive capacitive dilatometer. This is the first time that this technique has been applied to plutonium. Although our results were limited by access to material, our data is consistent with both a low temperature onset of Kondo coherence (a correlation effect that has been invoked to explain the non-magnetic states of plutonium) and a potential field-tuned phase change to the beta phase at higher temperatures, the latter increasing the challenge of interrogating the alpha phase electronic state. The data ultimately tell an interesting but as yet unresolved story of the interaction of electronic states, correlated behavior, and the influence of magnetic fields. We remain hopeful that such work will continue to shed even more light on this compelling mystery.

Acknowledgments

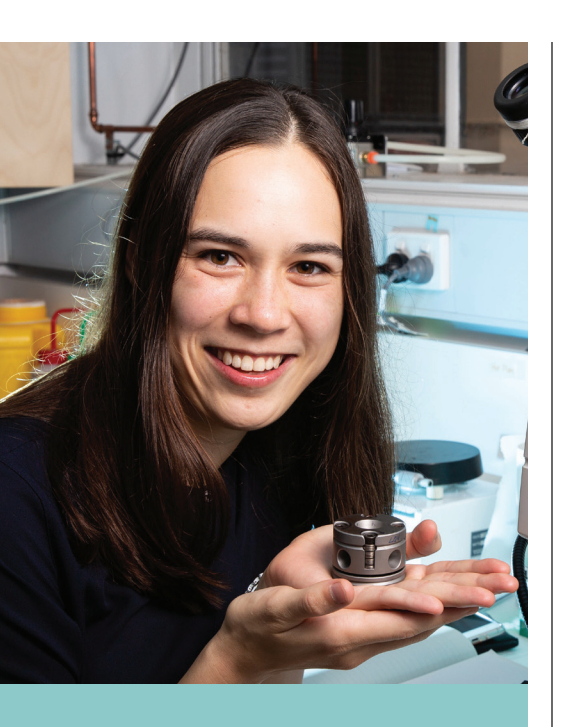
I'd like to thank my mentors Paul Tobash and Neil Harrison, in addition to the National High Magnetic Field Laboratory Pulsed Field Facility and MST-16 for their amazing assistance in this work, and the Seaborg Institute for making all this possible. Additional thanks to Franz Freibert and David Clark for their input in the writing of this article.

Further reading:

- J.C. Lashley, A. Lawson, R.J. McQueeney, G.H. Lander, "Absence of magnetic moments in plutonium," Phys. Rev. B, 2005, 72, 054416.
- 2. N. Harrison, J.B. Betts, M.R. Wartenbe, F.F. Balakirev, S. Richmond, M. Jaime, P.H. Tobash, "Phase stabilization by electronic entropy in plutonium," Nat. Commun., 2019, 10, 3159.
- 3. C. Tyler, "Magnetostriction," 1663, August 2020.
- 4. A.M. Boring, J.L. Smith, Los Alamos Science, 2000, 26, 90.







Larissa Huston

Larissa Huston was a Seaborg Institute Research Fellow in the Static High Pressure team in the Shock and Detonation Physics group at Los Alamos National Laboratory between 2019 and 2022. She now works at a research institute in Australia.

Actinides Under Extreme Pressures

Larissa Q. Huston

Commonwealth Scientific and Industrial Research Organisation (CSIRO), NSW, Australia.

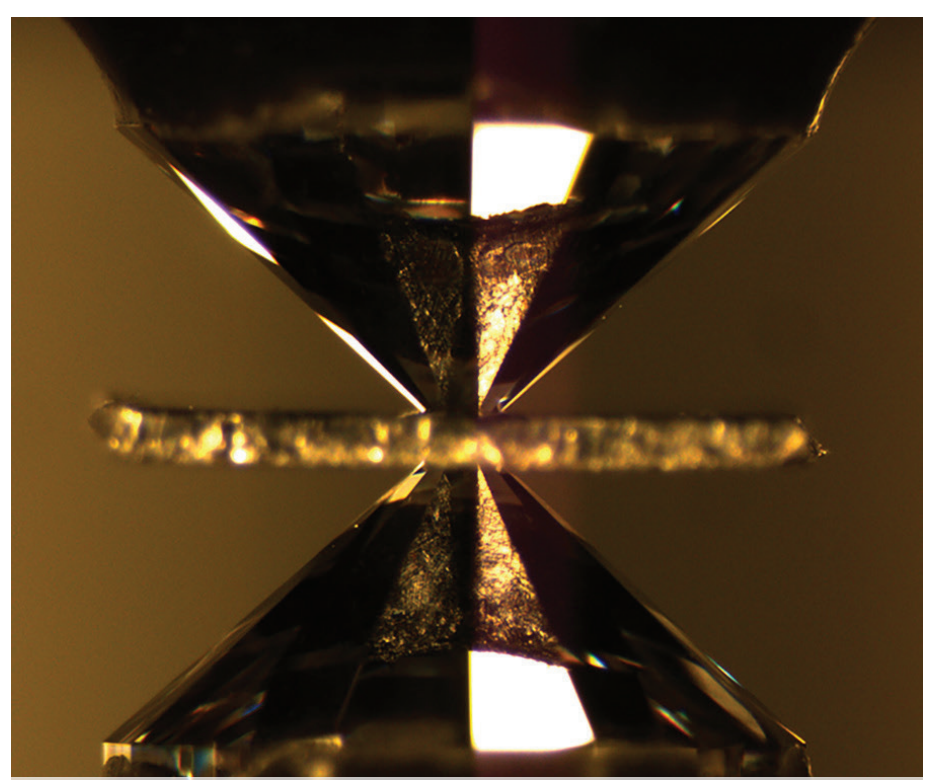
Applying high pressures to materials can induce profound effects on the electronic structure, bonding, and coordination environments of atoms. This can, in turn, be used to probe phenomena such as nonlinear optical properties, magnetism, superhardness, and superconductivity. In actinide and actinide compounds, the presence of itinerant or localized 5f electrons can create exotic material properties, including unconventional superconductivity, magnetism, hidden order, and heavy-fermion behavior. These properties can be particularly sensitive to the coordination environment, as actinide-actinide distances have a large effect on the behavior of 5f electrons. A comprehensive understanding of this behavior, however, is far from clear, and much more fundamental research remains to be done.

Uranium ditelluride (UTe₂) was recently found to display unusual superconducting properties that change with pressure. While the material is well characterized up to 2 GPa, its behavior at higher pressures is not currently well understood—in this work, we have investigated its behavior in this regime at high pressures up to 25 GPa.

Actinide bonding

For actinide elements, the distance between atoms plays an important role in defining the properties of the material. We observe this in changes in the metallic radii across the series (Fig. 1.; metallic radius is defined as half the average distance between atoms in the metallic state). The light actinides, such as protactinium, uranium, and neptunium, have a small metallic radius, allowing the 5f orbitals to overlap and the electrons to participate in bonding—known as itinerant behavior (Fig. 2). This results in low-symmetry structures, because when the 5f orbitals overlap they imprint their low symmetry on the structure. Heavy actinides with larger metallic radii, such as americium, curium, berkelium, and californium, meanwhile, have 5f orbitals that do not overlap. The electrons in these orbitals are localized, possess magnetic moments, and generally do not participate in bonding, much like the 4f lanthanides, resulting in high-symmetry structures. Note that plutonium is an exception and lies between these localized and itinerant behaviors; while the alpha phase behaves more like the light actinides (e.g., low-symmetry structure, small volume), the other phases (beta, gamma, delta prime, and epsilon) exhibit behaviors that straddle the boundary between 5f electron localization and itinerancy, with delta exhibiting the most localized 5f behavior. Surprisingly, it shows no magnetic ordering of localized magnetized moments (see p18 for more).

The nature of 5f electrons can be strongly affected by external variables like pressure and magnetic field, and also by alloying with other elements. In uranium intermetallic compounds (i.e., those containing uranium and metallic or semimetallic elements), small uranium-uranium distances typically give rise to itinerant 5f electrons and superconducting properties (e.g., U_6 Fe, U-18Mo), while large uranium-uranium distances typically have localized 5f electrons and undergo magnetic order (e.g., UCu_5 , USb_2). Uranium intermetallic compounds are also of technological importance in nuclear fuel chemistry (e.g., uranium-molybdenum alloys).



Two diamonds at the heart of the diamond anvil cell contain extremely small, parallel tips between which a sample is placed. Very large pressures, exceeding those at the center of the Earth, can be exerted using minimal compressive force. Credit: Steve Jacobsen, Northwestern University.

Uranium ditelluride

Uranium ditelluride is an intermetallic compound that was recently discovered to be a superconductor with a critical temperature of $T_{\rm c}$ = 2 K. It is proposed to be a topological superconductor, in which case its superconductivity could potentially be used as qubits for quantum computation. Superconductors typically have a critical magnetic field where superconductivity is destroyed—for uranium ditelluride, its critical magnetic field is unusually high at above 65 T. It also possesses multiple superconducting phases, which occur in different magnetic field directions, adding to its interest as a focus of study. When subjected to high pressure, another superconducting phase appears with increasing pressure above 0.3 GPa, with superconductivity disappearing completely at 1.6 GPa.

Some useful insight is gained by looking at the electronic structure of uranium ditelluride. Using X-ray absorption near-edge spectroscopy (XANES), researchers have found that the 5f electrons exist in a mixed-valence state at ambient pressure, with both uranium(IV) (f²) and uranium(III) (f³) configurations. These two states represent the itinerant-localized dichotomy: the f³ state is dominant at ambient pressure and shows itinerant character, whereas the minor f² component is localized. When uranium ditelluride is subjected to high pressure, the electrons become more localized, and superconductivity vanishes. This is unusual as higher pressure usually leads to more itinerant electrons (closer atomic distances and increased orbital overlap).

At ambient pressure, the crystal structure of uranium ditelluride is known to be orthorhombic with an *Immm* space group. We were interested in how this structure changes with pressure, and therefore chose to use diamond anvil cells coupled with angle-dispersive X-ray diffraction, which can be used to determine changes in crystal structure.

Reaching high pressures

A diamond anvil cell is a small but powerful device that is used to compress samples to ultrahigh pressures (a schematic is shown in Fig. 4). In a typical experiment, a sample is placed between two diamonds in a chamber that is made by drilling a hole in a metal gasket. The diamonds are held in place using seats made from cubic boron nitride, which is X-ray transparent, allowing X-rays to pass through. This optical transparency is a key factor that distinguishes the diamond anvil cell from other pressure devices, allowing material properties to be gauged while under compressive force. Increasing the pressure in a diamond anvil cell is achieved by pushing the diamonds together with opposed uniaxial force. Each diamond has a very small flat tip, known as a "culet," so that a minimal amount of force can be used to generate significantly high pressures. Pressures greater than those at the center of the Earth can be attained using the diamond anvil cell (approximately 360 GPa).

In this work, uranium ditelluride was compressed to 25 GPa, the pressure equivalent to approximately 400 miles underground, or about 10% of the distance to the center of the Earth. While subjected to these high pressures, the material was probed using X-ray diffraction. The size of the samples are comparable with the width of a human hair (diamond-tip diameters ranged from 150 to 400 μm in our experiments) and, therefore, it was imperative that we used an X-ray source with significantly higher intensity and focus than available in standard laboratory equipment. We turned to the Advanced Photon Source (APS) synchrotron at Argonne National Laboratory, which has a facility that specializes in high-pressure research: HPCAT (High-Pressure Collaborative Access Team). This is a world-class facility at the cutting edge of high-pressure research and has many close collaborations with scientists at Los Alamos National Laboratory.

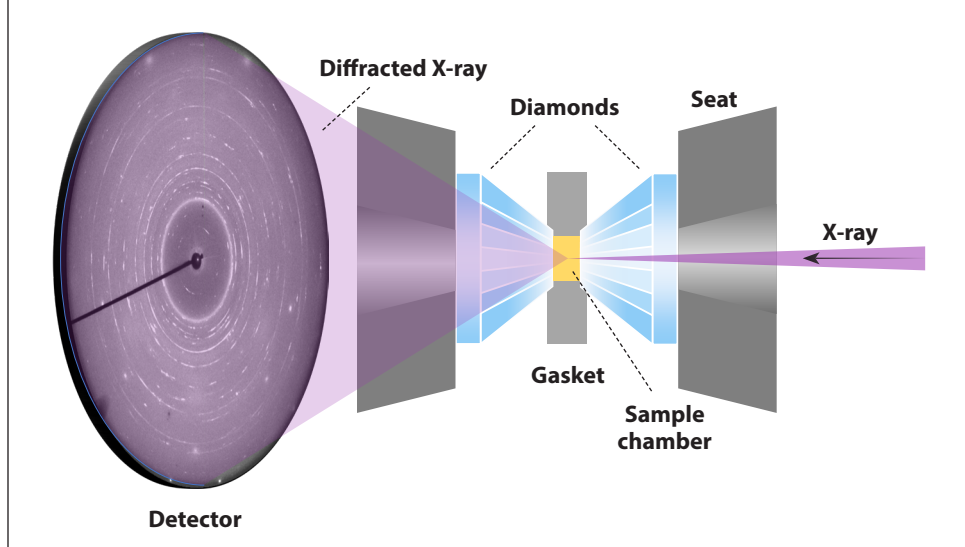


Figure 4. A schematic diagram of a diamond anvil cell setup. A sample is compressed between two diamonds and exposed to an X-ray beam.

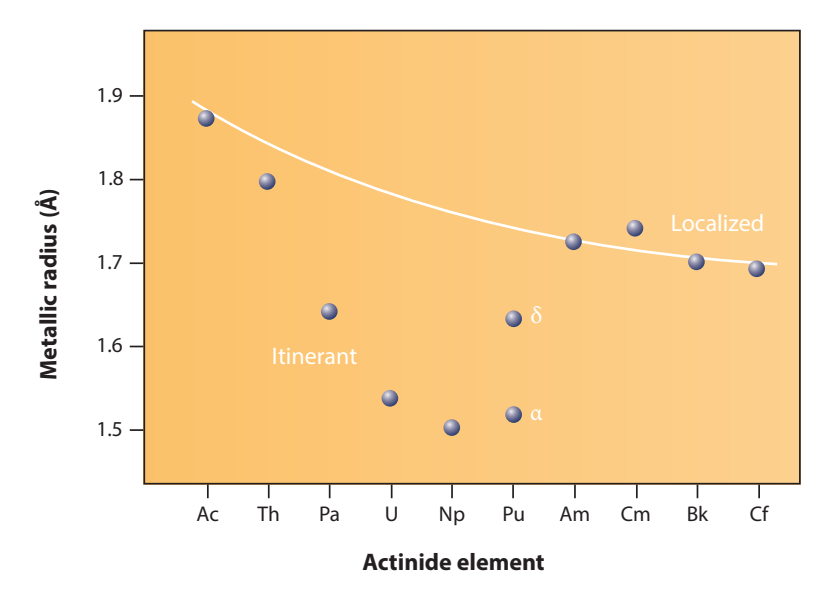


Figure 1. Metallic radii of the metallic actinide elements Ac–Cf in the ground state (spheres). The line meanwhile follows the smoothly varying metallic radii of the (+3) actinide ions, whose *f* electrons are localized and therefore nonbonding. The metallic radii of the light actinides (thorium to neptunium) fall on a parabolic curve below the trivalent line, showing the contribution of the *f*-electrons in the bonding—that is, pulling the atoms closer together. Plutonium meanwhile lies in between these two extremes: while the alpha phase behaves more like the light actinides, the other phases (beta, gamma, delta prime, and epsilon) exhibit behaviors that straddle the boundary between 5*f* electron localization and itinerancy, with delta exhibiting the most localized 5*f* behavior. Reproduced from Boring and Smith, Los Alamos Science, 2000, 26, 90.

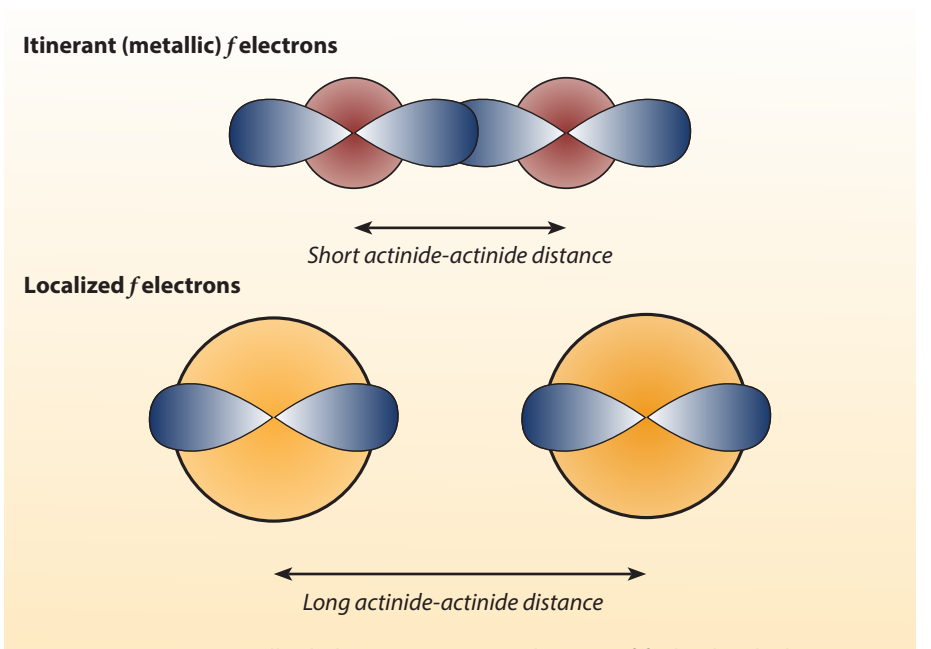


Figure 2. Itinerant (metallic) behavior requires overlapping of *f* orbitals, which in turn requires short actinide-actinide distances, allowing the electrons to move freely throughout the solid. This allows for superconducting properties in some uranium intermetallic species. Long actinide-actinide separations give rise to localized electrons, whose nonbonding nature can give rise to ordered magnetism.

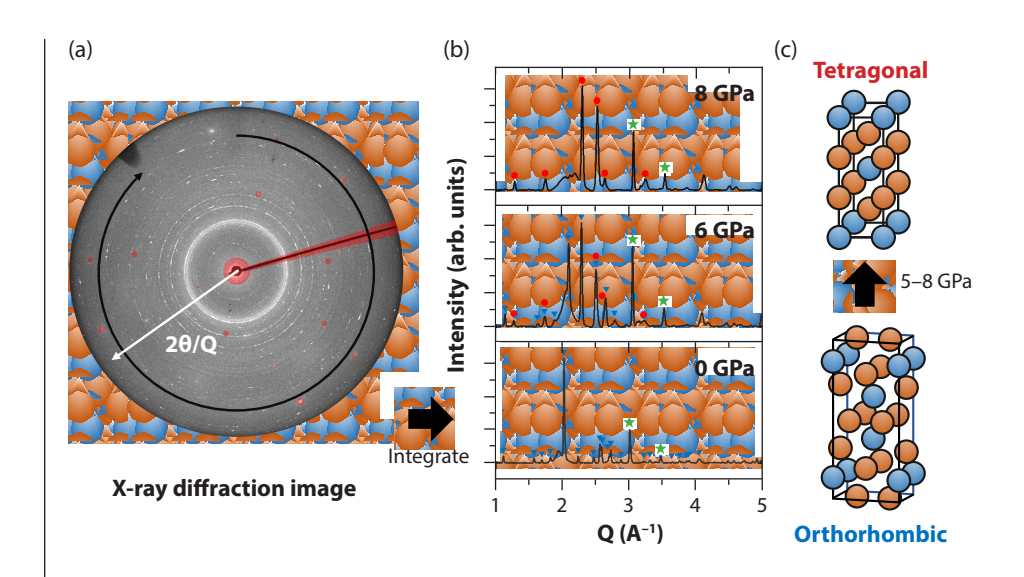


Figure 6. (a) An example of an X-ray diffraction pattern collected by passing X-rays though a diamond anvil cell. (b) The integrated diffraction patterns at three different pressures 0, 6, and 8 GPa; peaks labelled in blue triangles correspond to the orthorhombic structure, red circles correspond to the tetragonal structure. Additional peaks (green stars) are from the copper that was used to determine the pressure. (c) The orthorhombic and tetragonal structures of uranium ditelluride.

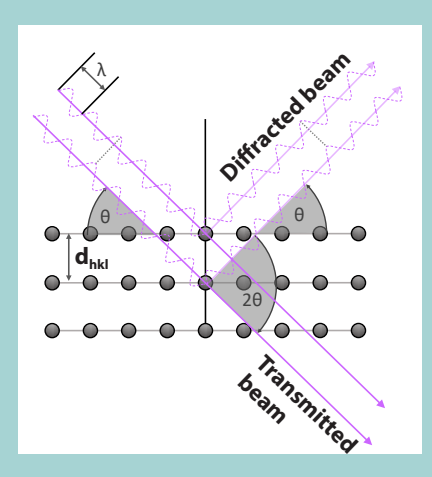


Figure 5. A schematic diagram of X-ray diffraction.

X-ray diffraction

X-ray diffraction can be used to determine the way atoms are arranged in a material in a repetitive 3D pattern—i.e., a crystal structure. In the case of uranium ditelluride, this allows for the density, uranium-uranium distance, and changes in the crystal structure to be determined. X-ray diffraction involves passing a beam of X-rays through a material and observing how the radiation scatters off the material. At an incidence angle θ , the reflected X-rays constructively interfere with X-rays that reflect off other parallel planes, strengthening these signals that can be measured. The scattering of X-rays is described using Bragg's law (see Fig. 4 for a diagram of the different variables).

The material studied is a powder constituted of multiple small particles which are oriented differently from each other. Each of these grains will therefore have different sets of parallel planes of atoms that satisfy Bragg's law. The angle of diffraction θ can then be used to determine the difference between atomic planes and calculate the crystal structure of uranium ditelluride. Different crystal structures will have different spacings between the parallel planes of atoms. This allows X-ray diffraction to be used to identify a crystal structure.

Uranium ditelluride under high pressure

An example of an X-ray diffraction image of uranium ditelluride in the diamond anvil cell is shown in Fig. 6a. This image is composed of multiple concentric rings with each ring representing a different set of parallel planes of atoms that diffracts X-rays at an angle of 20. Integrating these diffraction patterns around the rings gives the 1D diffraction patterns shown in Fig. 6b.

At 0 GPa, uranium ditelluride has an orthorhombic crystal structure, meaning that the atoms are arranged within a rectangular prism where all sides have different lengths and are perpendicular to each other. Fig. 6c shows how the uranium and tellurium atoms are arranged within the orthorhombic unit cell, where the unit cell is the repeating unit that makes up the crystal structure. Given that the dimensions of the unit cell are not equal, there are many different spacings between different parallel planes of atoms, resulting in a large number of peaks in the 1D diffraction pattern. The peaks corresponding to the orthorhombic structure are indicated by blue triangles in Fig. 6b.

When the pressure was increased to 6 GPa, the peaks from the orthorhombic structure decrease in intensity and additional peaks appear. These peaks indicate that the atoms in the orthorhombic structure have shifted positions to form a new crystal structure. In this case, the new crystal structure is a tetragonal structure with an *I4/mmm* space group, where the atoms repeat in a square prism unit cell with two equal and one unequal sides (Fig. 6c). At this pressure, both the orthorhombic and tetragonal structures are present. At 8 GPa, only the latter is present, meaning that all the atoms have rearranged themselves into the tetragonal structure. The new structure of uranium ditelluride remains present when pressure is decreased down to atmospheric pressure (this change in crystal structure is known as a phase transition). As the arrangement of atoms is different in the tetragonal phase, the uranium-uranium distance changes and therefore the interactions between the 5*f* electrons and the uranium atoms are different. The material slowly reverts to the orthorhombic phase approximately 2–3 weeks after being decompressed to ambient pressure.

Compressibility hints

The bulk modulus is a quantity that measures a material's resistance to being compressed. A material with a high bulk modulus such as diamond is difficult to compress while a material with a low bulk modulus such as a sponge is easier to compress. However, as a sponge is compressed, it becomes more difficult to further compress the smaller it becomes. This means that the bulk modulus changes in a material under compression, therefore, the change in bulk modulus with pressure is an important value to quantify.

When a material is compressed, its unit cell typically becomes smaller as atoms are pushed closer together, meaning that the same atoms occupy a smaller volume. The pressure-volume relationship can be modeled to give the bulk modulus and how it changes with pressure, known as an equation of state. If a bulk modulus is small, the volume decreases at a faster rate. The solid lines in Fig. 7 show the fit of the equation of state to the data. With this fit, we find that at ambient pressure (0 GPa), the orthorhombic phase shows a bulk modulus of 46 GPa, versus 79 GPa for the tetragonal phase. This means that at ambient pressure, the tetragonal phase is more difficult to compress than the orthorhombic phase.

Determining the bulk modulus is important because it can give us hints about why uranium ditelluride undergoes a phase transition at high pressure. This is due to the relationship between the bulk modulus, the complexity of the crystal structure (symmetry), and the bonding of the electrons. In compounds where the bulk modulus is lower for the low-pressure phase (e.g., uranium telluride, UTe), the change in crystallographic phase was explained by a mixed-valence state. The accompanying change in bulk modulus is due to this change in crystal structure—for example, graphite is soft and easy to compress but if you phase-transform it to diamond, it becomes difficult to compress. Uranium ditelluride has similar behavior to uranium telluride, where the phase which is more resistant to compression is observed, i.e., the one with a higher bulk modulus. In the case of uranium ditelluride, this is the tetragonal structure, suggesting that a mixed-valance state is present in orthorhombic uranium ditelluride, which has been reported in the literature.

A higher bulk modulus is also consistent with a simpler, higher symmetry structure (tetragonal is simpler than orthorhombic), with larger uranium-uranium distances. These distances change from 3.6 Å (low pressure, orthorhombic) to 3.9 Å (high pressure, tetragonal), and reflect increased 5f localization. Therefore, the bulk modulus provides further evidence for the transition to a simpler structure under pressure, and that this change in the mixed-valence state may be driven by localization of the 5f electrons.

"Uranium ditelluride was compressed to 25 GPa, the pressure equivalent to approximately 400 miles underground, or about 10% of the distance to the center of the Earth."

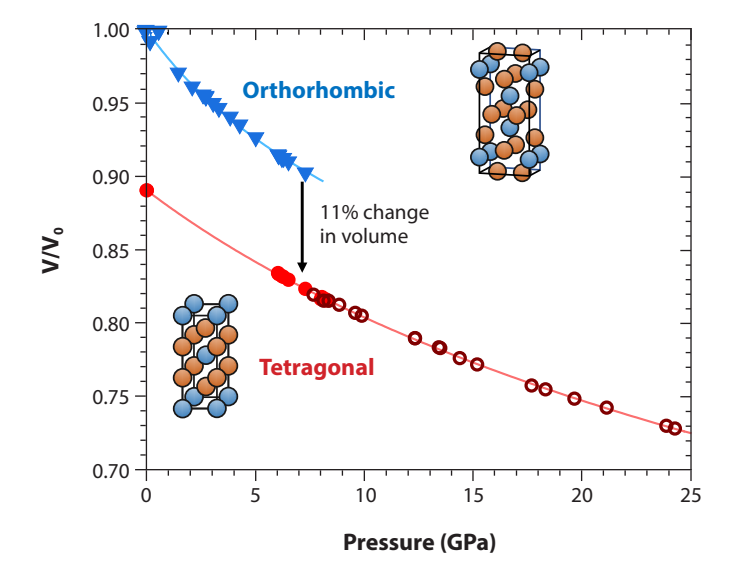


Figure 7. The relationship between pressure and volume of uranium ditelluride (V) with respect to the original volume (V_0) . The blue triangles show this relationship for the orthorhombic phase and the red circles show this relationship for the tetragonal phase. The solid lines show a fit to an equation of state model which relates pressure to volume.

Hill plots

Prior to 1970, researchers could not predict whether uranium compounds would be superconducting or magnetic. This all changed when Los Alamos scientist Hunter Hill discovered a simple empirical relationship for light actinide and cerium compounds—he found that the distance between *f*-element centers determines whether their ground states are superconducting or magnetic (Fig. 2). Remarkably, this was independent of the nature of any non-*f*-element atoms that separated them. Short interatomic distances give rise to itinerant, superconducting behavior, whereas long distances give localized, magnetic properties. Hill theorized that f electrons could hybridize

only with each other, so the closer the *f*-element centers were, the greater the ability to form superconducting bands. The intervening non-*f*-electron atoms were just spacers that served only to alter the degree of f-orbital overlap. The Hill plot was therefore a major step towards understanding the light actinides. Hill observed that superconductivity appeared predominantly at uranium-uranium distances < 3.4 Å (Hill limit, blue gradient in Fig. 2). However, subsequent discoveries of anomalous superconductors with large uranium-uranium separations did not fit in with this observation but are now understood to be part of a family of heavy-fermion superconductors (e.g., UBe₁₃ and UPt₃).

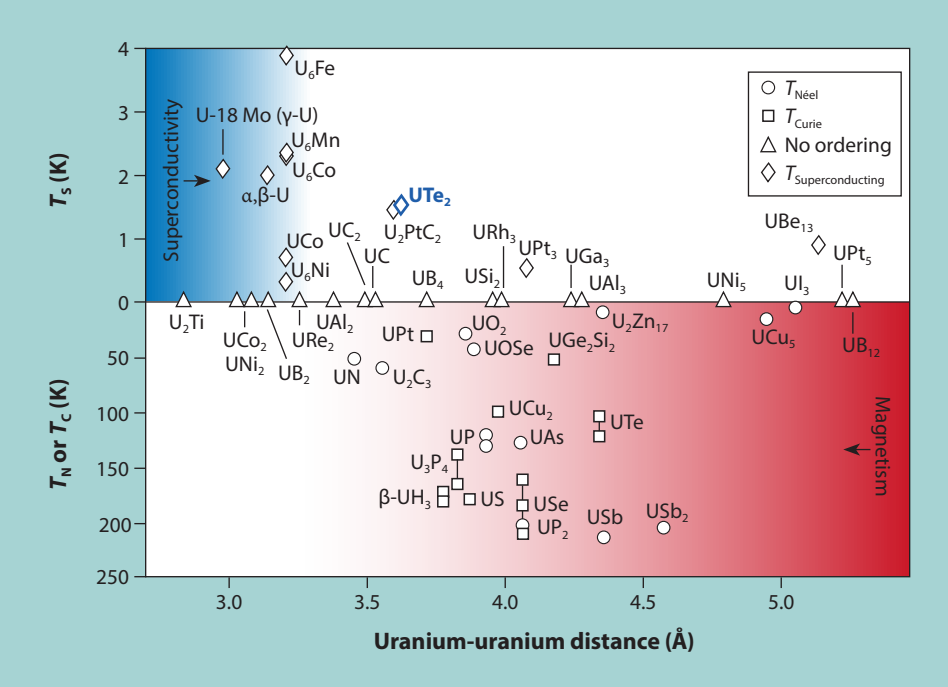


Figure 3. Hill plot for uranium compounds, showing the superconducting (T_s , diamonds) or magnetic transition temperatures (T_N or T_{Cr} circles or squares) versus interatomic spacing separating the f-element atoms. Note the superconducting heavy-fermion compounds UPt₃ and UBe₁₃ which fall outside of Hill's limit (in blue). Reproduced from Boring and Smith, Los Alamos Science, 2000, 26, 90.

Summary

High-pressure X-ray diffraction was performed on uranium ditelluride, a uranium intermetallic compound with recently discovered superconducting properties that vanish at high pressures. At these pressures, we found that it undergoes a phase transformation from its ambient orthorhombic structure to a tetragonal structure, beginning at 6 GPa and completing the transformation at 8 GPa. The difference in the bulk modulus of the two phases and the transition to a simpler crystal structure with greater uranium-uranium distances and high symmetry suggests that the phase transition is likely due to an increased localization of the 5*f* electrons.

Acknowledgments

Funding of this work was provided by the Seaborg Institute. Beamtime access was provided by the High-Pressure Collaborative Access Team (HPCAT) at Argonne National Laboratory, which is funded by the DOE and NNSA. The author would like to thank Blake Sturtevant and Eric Bauer for their mentorship and Priscilla Rosa, Ashley Weiland, Brian Scott, and Dmitry Popov for their contributions to this work.

Further reading:

- L.Q. Huston, D.Y. Popov, A. Weiland, M.M. Bordelon, P.F.S. Rosa, R.L. Rowland, II, B.L. Scott, G. Shen, C. Park, E.K. Moss, S.M. Thomas, J.D. Thompson, B.T. Sturtevant, E.D. Bauer, "Metastable phase of UTe₂ formed under high pressure above 5 GPa," Phys. Rev. Materials, 6, 2022, 114801.
- 2. S.M. Thomas, F.B. Santos, M.H. Christensen, T. Asaba, F. Ronning, J.D. Thompson, E.D. Bauer, R.M. Fernandes, G. Fabbris, P.F.S. Rosa, "Evidence for a pressure-induced antiferromagnetic quantum critical point in intermediate-valence UTe₂" Sci. Adv., 6, 2020, eabc8709.
- 3. J.A. Mydosh, P.M. Oppeneer, "Hidden order behaviour in URu₂Si₂," Philos. Mag., 94, 2014, 3642.
- 4. F.B. Santos, M.H. Christensen, T. Asaba, F. Ronning, J.D. Thompson, E.D. Bauer, R.M. Fernandes, G. Fabbris, P.F.S. Rosa, "Evidence for a pressure-induced antiferromagnetic quantum critical point in intermediate-valence UTe₂" Sci Adv., 6, 2020, eabc8709.
- 5. N. Shekar, V. Kathirvel, B. Shukla, P. Sahu, "Phase transitions and structural stability of binary uranium intermetallics under high pressure: A review," Proc. Natl. Acad. Sci. India A, 82, 2012, 163.
- J.M. Léger, I. Vedel, A.M. Redon, J. Rossat-Mignod, O. Vogt, "High pressure X-ray studies of UAs and UTe," Solid State Commun., 66, 1988, 1173.
- 7. S. Ran, S.R. Saha, I.L. Liu, D. Graf, J. Paglione, N.P. Butch, "Expansion of the high field-boosted superconductivity in UTe₂ under pressure," npj Quantum Mater., 6, 2021, 75.
- 8. S. Ran, C. Eckberg, Q-P. Ding, Y. Furukawa, T. Metz, S.R. Saha, I-L. Liu, M. Zic, H. Kim, J. Paglione, N.P. Butch, "Nearly ferromagnetic spin-triplet superconductivity," Science, 365, 2019, 684.
- 9. A.M. Boring, J. Smith, "Plutonium condensed-matter physics," Los Alamos Science, 26, 2000, 90.

Phosphorus-Containing Ligands Support f-Block Complexes

Stephanie H. Carpenter

Los Alamos National Laboratory (LANL) has a long history of working with the transuranic elements. Since the Laboratory's inception, LANL has been at the forefront of actinide research, creating advancements in areas such as nuclear fuel processing, medical isotopes, and coordination chemistry for molecular actinide complexes. Despite continued progress in actinide chemistry, our fundamental knowledge of the electronic structure and bonding properties of molecular actinide complexes lags significantly behind our understanding of their transition metal counterparts. This is because of the technical challenges associated with the radioactive actinides. To address this gap in understanding, a sustained effort has been made to generate new structural motifs to explore the bonding properties of molecular f-block compounds. Through deliberate ligand design, a series of complexes can be generated to compare properties of lanthanide and actinide metal compounds (e.g., oxidation states, structural motifs, magnetic properties) under similar coordination environments. These studies explore the use of a bidentate ligand system, bis(acyl)phosphide (BAP), with lanthanides and actinides for electronic structure and bonding comparisons.

Ligand design and synthesis

BAP ligands are a molecular class of phosphorus complexes typically used as precursors for synthesizing industrial photoinitiators. Upon coordination to a metal center, BAP ligands are expected to behave as bidentate, anionic supporting moieties. This ligand class should provide stabilization through the electronically and geometrically flexible phosphorus atom in the backbone of the ligand, which would also act as a versatile spectroscopic handle (phosphorus-31, spin 1/2). A significant advantage to using these ligands is their facile synthesis from accessible, low-cost materials (Fig. 1). BAP compounds are easily tunable by substituting the acyl chloride used in ligand synthesis, allowing for variations with increased or decreased steric bulk. Despite the potential advantages of BAP ligands in metal chemistry, their use in coordination chemistry is rare for metals and unknown for *f*-block elements. We hypothesized that BAP ligands could stabilize a series of molecular *f*-block complexes with new molecular motifs and oxidation states.

Using metal series to investigate bonding trends

The radiological concerns and technical challenges of performing research with transuranic elements require rigorous studies with surrogate metals to fully understand the molecular system. Lanthanide metals are often employed as surrogates for the more radioactive transuranic elements given their similar size and reactivity, and as a consequence, the more rigorous and less hazardous lanthanide studies take far longer than analogous, more selective actinide investigations. Our fundamental study into the bonding interactions of actinide BAP complexes therefore began with the lanthanide metals. We hypothesized europium (Eu) and erbium (Er) would provide access to unusual reactivity and magnetic properties while simultaneously serving as surrogates for actinide metals.



Stephanie Carpenter

Stephanie joined LANL in November 2019 under the mentorship of Aaron M. Tondreau and Ping Yang. She was a Seaborg Institute Postdoctoral Fellow from August 2020 to June 2022. Stephanie is interested in the synthesis of molecular actinide and transition metal complexes and understanding the complex electronic structure of these complexes via numerous spectroscopic techniques. She is currently a scientist in the Stockpile and Enterprise Analytics Office, focusing on data analysis for enterprise-wide problems.

$$\begin{array}{c} \text{Na, } 10\% \text{ C}_{10}\text{H}_8 \\ \text{tBuOH} \\ \\ \text{P}_{\text{red}} & \longrightarrow & \text{NaPH}_2(\text{NaO}^{\text{t}}\text{Bu})_x \\ \\ \text{dimethoxyethane} & x = 2.4-2.8 \\ \\ \text{NaPH}_2(\text{NaO}^{\text{t}}\text{Bu})_x & \longrightarrow & \text{Mes} \\ \\ \text{NaPH}_2(\text{NaO}^{\text{t}}\text{Bu})_x & \longrightarrow & \text{NaPH}_2(\text{NaO}^{\text{t}}\text{Bu})_x \\ \\ \text{N$$

Figure 1. Example of Na-BAP ligand synthesis using mesitoyl chloride in the formation of sodium bis(mesitoyl)phosphide (Na(mesBAP)). The addition of tert-butanol results in the formation of NaPH₂ aggregates (1), where the subsequent addition of two equivalents of an acyl chloride results in the formation of Na-BAP ligands (2).

Ar = 2.4.6-trimethylphenyl (mes) or 2.4.6-triisopropylphenyl (tripp)

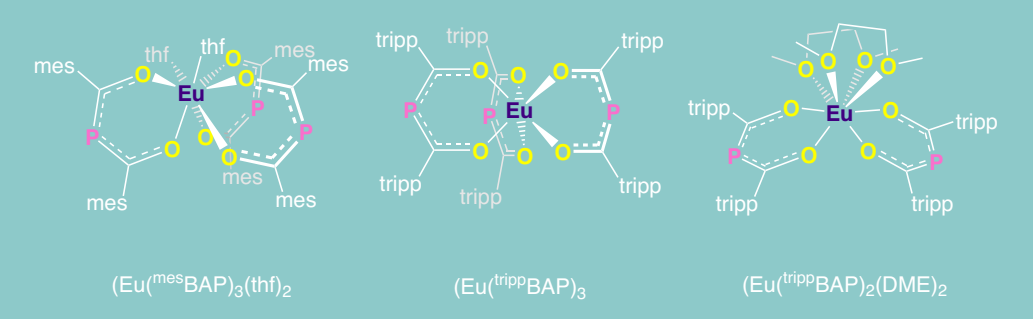


Figure 2. Synthesis of a series of europium (Eu) BAP complexes, resulting in two europium(III) complexes $(Eu(^{mes}BAP)_3(thf)_2, thf = tetrahydrofuran, and <math>Eu(^{tripp}BAP)_3)$ and one europium(II) complex $(Eu(^{tripp}BAP)_2(dme)_2, dme = 1,2-dimethoxyethane)$.

$$+1$$
 electron $+1$ electron

Figure 3. $Er(tripp BAP)_3$ can be reduced by either one or two electrons to isolate the three-electron series.

Initial studies sought to probe the reactivity of two BAP ligands towards europium, resulting in a series of closely related molecular europium BAP complexes. Europium is known to have unique magnetic properties due to its large magnetic moment associated with the 4f7 electron configuration, therefore, a series of europium complexes with varying oxidation states could provide insight into the molecules' electronic structures. The coordination number (the number of ligand donor atoms bound to the metal center) of europium BAP complexes depends on the size of the BAP ligand. Using the mesitoyl-phosphide derivative (mesBAP) and the larger triisopropylbenzoyl-substituted (trippBAP) anionic ligands, we obtained the respective europium(III) complexes bearing three ligands (Fig. 2). The coordination number of these two complexes differed due to the steric demands imparted by the two different types of ligands. We hoped to compare this ligand motif with varying europium oxidation states, though europium(II) complexes are prone to dimerization. The larger trippBAP moiety was used to avoid potential dimerization and generate a europium(II) complex with two ligands. Variable temperature magnetic susceptibility measurements for the three europium BAP complexes revealed no unusual behavior for any of the metal centers.

Initial europium studies showed the feasibility of using the BAP motif to stabilize molecular lanthanide complexes over multiple oxidation states. Encouraged by these results, further investigations into the reactivity of the ^{tripp}BAP moiety were performed with erbium, a lanthanide metal with a spin-active nucleus that provides an additional spectroscopic handle for characterizing and understanding the electronic structures of these compounds. After successfully synthesizing an erbium(III) complex with three ligands, $Er(^{tripp}BAP)_3$, reduction by one or two electrons allowed for the formation of new complexes in the formal oxidation states of erbium(II) and (I) (Fig. 3). Magnetic studies to confirm these oxidation states are ongoing and it is likely that these formally designated oxidation states do not capture their true, complex electronic structures. Nevertheless, the electronic flexibility imparted by the ligand through the phosphorus atom in the backbone may provide electronic stabilization of formal oxidation states that are unprecedented for erbium.

Transuranic elements are only available in milligram quantities and working on these scales often provides challenges in the laboratory. In anticipation of these challenges, we attempted to prepare europium- and erbium-BAP complexes on

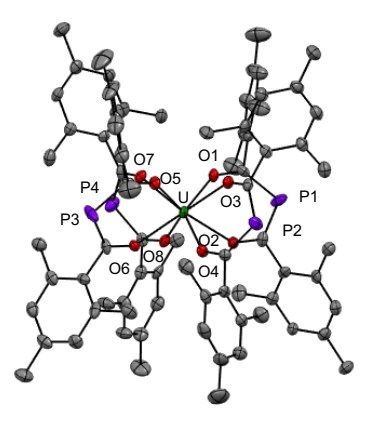


Figure 4. Solid-state structure of $U(^{mes}BAP)_4$ as determined by X-ray crystallography, with ellipsoids shown at 50% probability. Hydrogen atoms have been removed for clarity.

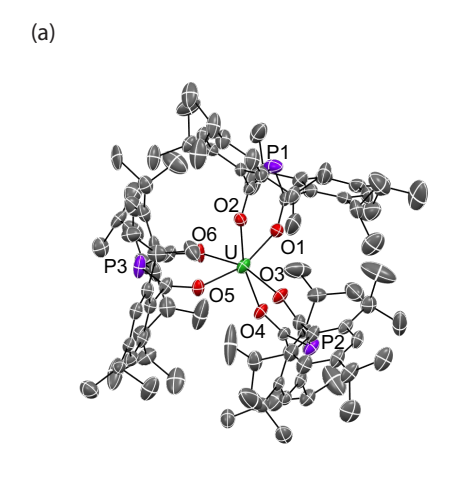
similar scales, and were successful using approximately 5 mg of metal content of europium and erbium starting materials. These encouraging results supported the viability of our proposed reactivity studies with BAP ligands and uranium and the transuranic elements.

Molecular uranium BAP complexes

The successful preparation of both the europium and erbium BAP series on a small scale allowed us to adapt this synthesis to uranium. We hypothesized the addition of the ^{mes}BAP ligand to uranium(III) iodide in a 3:1 ratio would result in the formation of a uranium(III) complex, which would be ideal for electronic structure studies via electron paramagnetic resonance (EPR) spectroscopy. Unfortunately, uranium is prone to single electron chemistry and ligand rearrangement, often resulting in the formation of unexpected compounds. As such, this reactivity led to the isolation of a uranium(IV) complex with four ligands, U(^{mes}BAP)₄, which was consistently and reproducibly isolated with no observed formation of the desired uranium(III) complex, despite the 3:1 stoichiometry of ligand to metal.

The mesityl groups on the mesBAP ligands are directed away from the large, reactive uranium center (Fig. 4), providing little steric protection and allowing for the unwanted formation of a uranium(IV) complex from uranium(III) starting materials. To mitigate undesired ligand rearrangement and disproportionation reactivity, we reasoned the increased steric bulk in trippBAP would limit the number of ligands bound to the uranium center and stabilize the desired uranium(III) complex. The analogous reaction using trippBAP (with a 3:1 ratio of ligand to uranium) successfully yielded the formally trivalent uranium complex, U(trippBAP)3.

Electronic structure studies employing a combination of single-crystal X-ray diffraction, EPR, nuclear magnetic resonance, and UV/vis./near-infrared spectroscopies suggest a complicated electronic structure for $U(^{tripp}BAP)_3$ beyond the expected simple uranium(III) ion. Solid-state metrical parameters suggest $^{tripp}BAP$ may be able to accept a significant amount of electron density, whereas EPR studies of $U(^{tripp}BAP)_3$ reveal a signal that does not significantly shift from the spin-only value of a free



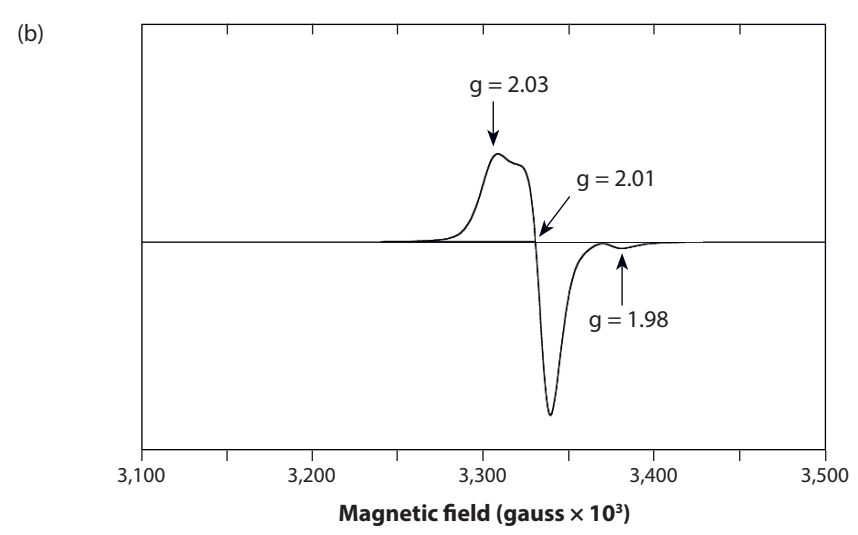


Figure 5. (a) Solid-state structure of U(trippBAP)₃ with ellipsoids shown at 50% probability. Hydrogen atoms have been removed for clarity. (b) Solid-state X-band electron paramagnetic resonance (EPR) spectrum of U(trippBAP)₃ taken at 10 K, 9.38 GHz. Average g-values are shown, and do not differ significantly for the spin-only value of a free-electron.

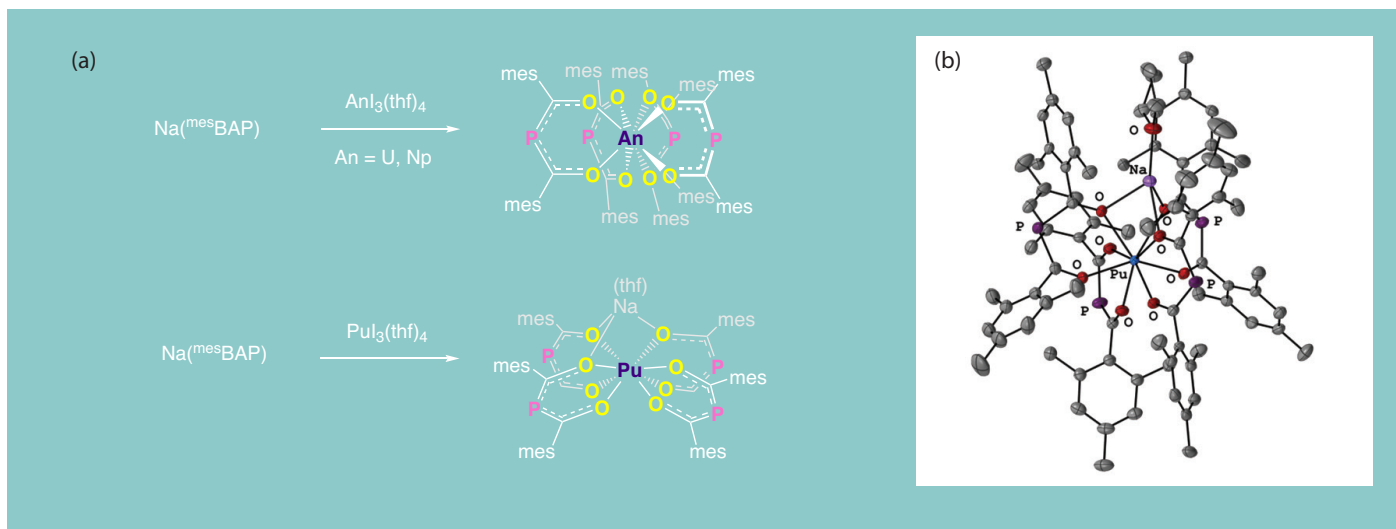


Figure 6. (a) Summary of the reactivity observed between ^{mes}BAP and the actinide series $Anl_3(thf)_4$ (An = uranium, neptunium, plutonium). (b) Solid state structure of $[Na(thf)][Pu(^{mes}BAP)_4]$ as determined by single crystal X-ray diffraction, with ellipsoids shown at 50% probability. Hydrogen atoms have been removed for clarity.

electron (Fig. 5). This observation suggests $U(^{tripp}BAP)_3$ has an unpaired electron in a molecular orbital containing both metal and ligand character, where the uranium center appears more as a uranium(IV) ion with an electron delocalized on the ligand. The disappearance of the EPR signal at room temperature further supports this observation. Rather than assuming electron placement on the metal or on the ligand, we feel the electronic structure studies of $U(^{tripp}BAP)_3$ suggest the uranium center exists on a continuum between the (III) and (IV) oxidation states.

Transitions into transuranic elements

Because both the lanthanide and uranium BAP complexes were accessible on a small scale (approximately 5 mg metal), we were encouraged that this chemistry could be adapted to the transuranic elements, specifically neptunium (Np) and plutonium (Pu). Neptunium is the most accessible transuranic metal and has unique reactivity—arising from its electronic properties—that remains poorly understood compared to uranium. Plutonium, meanwhile, exists as an outlier in the transuranic series studied, as it retains a high affinity for oxygen coordination yet is less prone to spontaneous oxidation to the tetravalent oxidation state compared to uranium and neptunium. By comparing homologous reactivity between these metals with mesBAP, we could directly contrast the effect of these elemental traits on the outcomes of reaction products. For mesBAP chemistry in particular, a motivation for the work was the hope of observing an outlier in the reaction series using plutonium starting materials. Fundamental reactivity investigations involving uranium, neptunium, and plutonium are rare, but Los Alamos is primed to lead the field of molecular actinide chemistry by encouraging these types of studies.

The neptunium BAP study examined the reactivity of mesBAP with a 3:1 ratio of ligand to neptunium starting materials in a reaction designed to closely mimic the conditions used for $U(^{mes}BAP)_4$. The product was identified as $Np(^{mes}BAP)_4$ using single-crystal X-ray diffraction, showing homologous reactivity between uranium and neptunium, where an unanticipated single electron event occurs and the product arises from spontaneous oxidation. The isolation of a neptunium(IV) complex shows the adaptability of this ligand set towards transuranic elements and highlights some of

Actinide Research Quarterly

the challenges when attempting to design ligands and reactivity specific to individual actinides. Current studies focus on exploring the electronic structure of Np(mesBAP)₄ using EPR spectroscopy, with initial analysis suggesting that the unpaired electrons, as expected, are found localized around the metal center.

The addition of mesBAP in a 3:1 ratio of ligand to plutonium starting material, homologous to the uranium and neptunium reaction conditions, gave rise to a unique product. Four mesBAP ligands were observed around the plutonium center, but a sodium atom from the ligand was found bound to the ligand oxygen atoms, leading to the assignment of a plutonium(III) oxidation state (Fig. 6). This result highlights the unique properties of plutonium, compared to uranium and neptunium, that give rise to behavior distinct from other actinide metals. Our approach to synthesis in this investigation is also important: by performing reactions in a series using related elements, ligands, and oxidation states, a stronger understanding of nuanced chemical behavior can emerge.

Summary

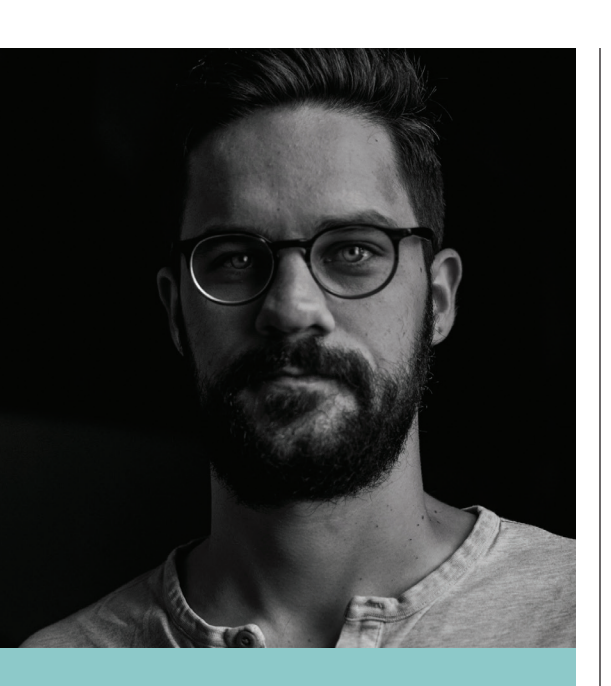
Bis(acyl)phosphide (BAP) ligands show unique reactivity towards uranium and neptunium, resulting in unexpected electronic structure assignments of the first isolated actinide BAP complexes. Spectroscopic investigations suggest the ^{tripp}BAP moiety can accept an appreciable amount of electron density that raises questions over accompanying metal oxidation states. The combined reactivity and magnetism studies of BAP ligands with europium, erbium, and uranium provide the foundation and context of this system while pushing the chemistry forward to neptunium and other transuranic elements. This knowledge can be used for the continued development of waste remediation, metal recycling efforts, and furthering our understanding of the chemical reactivity of plutonium.

Acknowledgments

This work is a collaborative effort with several other researchers: Nikki J. Wolford, Jesse Murillo, Ju Chen, Brennan S. Billow, Taylor V. Fetrow, Nathalia Cajiao, Joshua Mengell, Michael T. Janicke, Andrew J. Gaunt, Michael L. Neidig, Martin L. Kirk, and Aaron M. Tondreau were all critical to the progress and understanding of this project. Financial support was provided by the U.S. Department of Energy through the Office of Basic Energy Science and the Heavy Element Chemistry program (HEC@ LANL, 2020LANLE372, DE-AC52-06NA25396) and the Seaborg Institute for the postdoctoral fellowship of Stephanie H. Carpenter.

Further reading:

- 1. S.H. Carpenter, N.J. Wolford, B.S. Billow, T.V. Fetrow, N. Cajiao, A. Radović, M.T. Janicke, M.L. Neidig, A.M. Tondreau, "Homoleptic Uranium-Bis(acyl)phosphide Complexes," Inorg. Chem., 2022, 61, 32, 12508.
- 2. J. Chen, S.H. Carpenter, T.V. Fetrow, J. Mengell, M.L. Kirk, A.M. Tondreau, "Magnetism Studies of Bis(acyl) phosphide-Supported Eu3+ and Eu2+ Complexes," Inorg. Chem. 2022, 61, 46, 18466.
- 3. A. Huber, A. Kuschel, T. Ott, G. Santiso-Quinones, D. Stein, J. Bräuer, R. Kissner, F. Krumeich, H, Schönberg, J. Levalois-Grützmacher, H. Grützmacher, "Phosphorus-Functionalized Bis(acyl)phosphane Oxides for Surface Modification," Angew. Chem. Int. Ed. 2012, 51, 4648.
- 4. A. Eibel, M. Schmallegger, M. Zalibera, A. Huber, Y. Bürkl, H. Grützmacher, G. Gescheidt, "Extending the Scope of Bis(acyl)phosphane Oxides: Additional Derivatives," Eur. J. Inorg. Chem., 2017, 2017, 2469.
- 5. D.S. Michael and G. Schreckenbach, "Bis(acyl)phosphide Complexes of U(III)/U(IV): A Case of a Hidden Redox-Active Ligand," Inorg. Chem., 2024, 63, 21, 9711-9714.
- 6. S.H. Carpenter, J. Mengell, J. Chen, M.R. Jones, M.L. Kirk, A.M. Tondreau, "Determining the Effects of Zero-Field Splitting and Magnetic Exchange in Dimeric Europium(II) Complexes," Inorg. Chem., 2024, 63, 19, 8516-8520.



Zach Jones

Originally from Portland, Oregon, Zach received a BS in chemistry while conducting undergraduate research on inorganic solid-state superconducting materials with Prof. David *Johnson at the University of Oregon. Zach then attended the University* of California, Santa Barbara for his PhD work, probing structureproperty relationships of nanoscale heterogeneous catalysts with Prof. Susannah Scott. During one of his many synchrotron trips at the Stanford Synchrotron Radiation Lightsource, Zach met Stosh Kozimor, which led to the postdoctoral position and research described herein. Zach is now a Scientist in Sigma division with Fabrication Manufacturing Science (Sigma-1).

Advancing Understanding of Actinides in Aqueous Media

Zach Jones

Advancing our understanding of actinides in aqueous media could help solve many outstanding problems in actinide science. Almost all aspects of technologically relevant actinide chemistry rely—at some point—on aqueous actinide processing. The impact spans from large-scale plutonium metal production to actinide environmental monitoring and efforts to achieve energy security using nuclear power. Unfortunately, we have a real knowledge gap in this area—in particular, speciation and reactivity of actinides in industrially relevant aqueous solutions is often poorly defined. One example is actinide species dissolved in buffered ammonium acetateacetic acid solutions—beyond a few focused studies, this commonly used stock solution is poorly characterized because of the inherent challenges associated with handling highly radioactive actinides. Interpreting spectroscopic results from actinides in this complicated aqueous environment is also challenging compared to well-defined organic solutions and solid-state crystals. Nevertheless, the absence of knowledge in this area is surprising given that actinide-containing ammonium acetate-acetic acid solutions facilitate small-scale production of actinide metals, serve as starting materials for labeling chelators with alpha-emitting radionuclides for therapeutic applications, and are used in both aqueous synthesis and, to a more limited extent, actinide separations.

To explore actinide speciation in buffered ammonium acetate-acetic acid (pH=5.5) stock solution starting materials, we chose environments where the solvent mixture was present at three different concentrations. Our intent was to obtain results that were directly relevant (or easily extrapolated) to current uses in the laboratory. These three different concentrations were dilute (0.1 M), intermediate (4 M), and concentrated (15 M). In the dilute solution, the actinide and acetate ions were solutes in an aqueous matrix, while in the intermediate solution, there was an abundance of coordinating acetate ions in an excess of water. In the concentrated solutions, however, water was of sufficiently low concentration that it was a solute rather than a solvent. The primary analytical method that we used was solution-phase X-ray

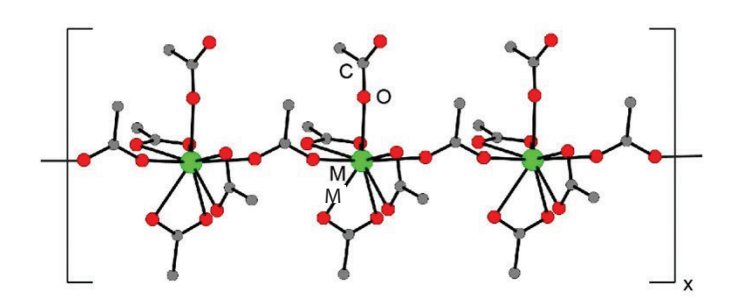


Figure 1. A ball and stick representation of the $(NH_4)_2M(acetate)_5$ $(M^{3+} = Eu, Am, Cm)$ structures obtained by single crystal X-ray diffraction.

Figure 2. Simulated scattering paths used to model the Ac³⁺ and Cm³⁺ L₃-edge EXAFS data. Single scattering and directly bound oxygen (orange and dark blue) and carbon (purple) were modeled for the first shell. The higher-order features were modeled with a triangle multiple scattering path (dark red), and a linear scattering path from the methyl backbone (yellow).

• • •

absorption spectroscopy (XAS), and we evaluated the results using structural data from single crystals grown from the acetate solutions. This included characterization of $M(acetate)_5^{2-}$ (M=americium, curium, and europium; the latter is a nonradioactive surrogate for the exploratory studies) using single-crystal X-ray diffraction.

For the X-ray absorption spectroscopy experiments, we examined two actinides on either end of the scale in the actinide series, in which ions get progressively smaller with increasing atomic number (known as the actinide contraction). Specifically, we chose the largest trivalent 5*f* element, actinium (Ac³+, ionic radius of 1.12 Å in six-coordinate complexes), and, in the middle of the series, curium (Cm³+, ionic radius of 0.97 Å in six-coordinate complexes), one of the smallest actinides that can be reasonably obtained in milligram quantities. By choosing these elements, we could examine the effect of actinide cation size, and by extension Lewis acidity, on coordination chemistry in these solutions.

Crystal structures

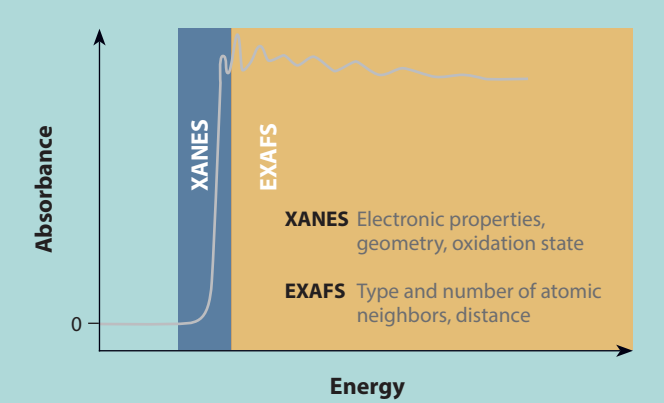
Solid-state structures of Am(acetate) $_5^{2-}$, Cm(acetate) $_5^{2-}$, and Eu(acetate) $_5^{2-}$ were isolated from slow evaporation of the trivalent metal cations dissolved in a 10 M aqueous solution of ammonium acetate. The M(acetate) $_5^{2-}$ compounds were isomorphous (crystallized in the same form; Fig. 1) with three bidentate, terminal acetate ligands (coordinated in two positions), one monodentate and terminal (bound in one location), and one monodentate and bridging. This gives an overall nine-coordinate geometry with no bound water molecules.

X-ray absorption spectroscopy

To determine if the solid-state structures were maintained in solution, we used the complimentary techniques of L_3 -edge X-ray absorption near edge spectroscopy (XANES) and L_3 -edge extended X-ray absorption fine structure (EXAFS) spectroscopy. X-ray absorption spectroscopy is well suited to characterize actinides in solution because it is atom-specific and provides information on oxidation state(s) and local structure even with very low concentrations of metal analytes (micrograms

X-ray absorption spectroscopy

X-ray absorption spectroscopy (XAS) is used to determine the local atomic structure and electronic states within a substance. Typically performed with synchrotron radiation, which offers high energy and tunable X-rays, XAS allows for precise examination of local structure, providing insights not available with traditional X-ray diffraction methods, and is applicable to a wide range of materials, including amorphous solids and solutions. When an atom absorbs an X-ray photon, it can either excite a core electron to a higher energy level or expel it entirely (electrons emitted like this are called photoelectrons). The wavelength of the absorbed photon indicatives the characteristics of the core electron. Peaks in absorbance, known as "edges," occurring at distinct wavelengths, yield valuable insights into the electron's properties. When scanning X-ray radiation energy through the range of interest, a distinct surge in absorption appears, indicating the absorption of an X-ray photon by a core electron. Termed the absorption edge due to its shape in the spectrum, it is labeled based on the principal quantum number of the excited electron (Table 1).



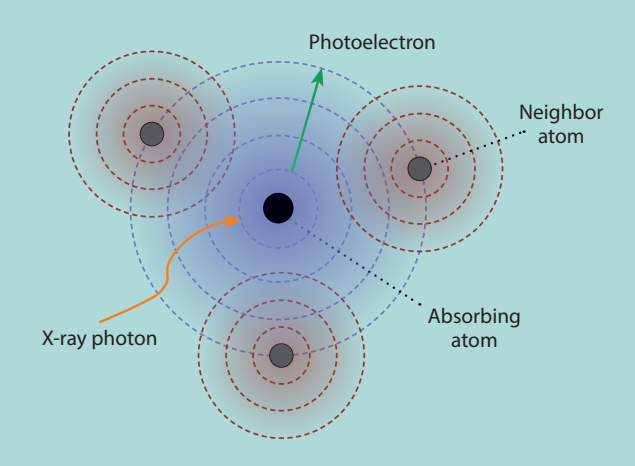
Above: The two main regions in an XAS spectrum—XANES and EXAFS.

Absorption edge	e Core shell			
K edge	1s			
L edge	2s	2p		
M edge	<i>3s</i>	<i>3p</i>	3d	
N edge	4s	4p	4d	4 <i>f</i>

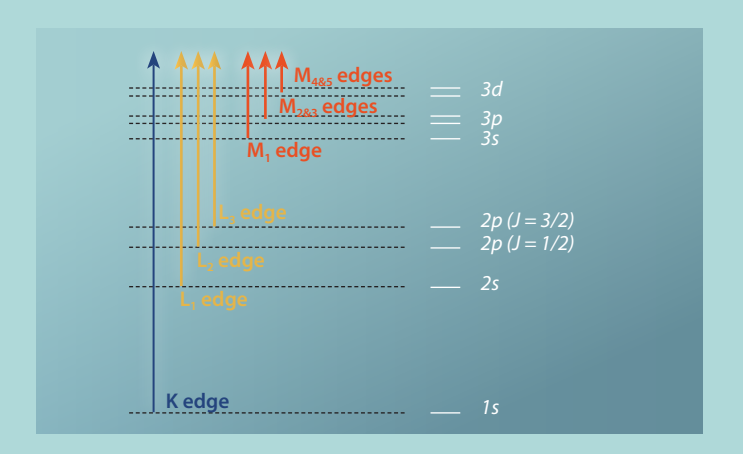
Table 1: Labels for the absorption edges correspond to the principal quantum number of the excited core electrons. Represented visually, *right*.

X-ray absorption near edge structure (XANES) refers to the spectroscopic structure found in the immediate vicinity of the absorption edge. XANES spectra serve as fingerprints that provide information about the electronic structure, including details about chemical bonding and oxidation state. Nonetheless, these details can be difficult to determine and pose challenges due to the effect of multiple scatterings by photoelectrons and auger electrons.

The region in the spectrum beyond the initial absorption edge is known as extended X-ray absorption fine structure (EXAFS). The term "fine structure" refers to the oscillations observed in the spectrum beyond the absorption edge, which arise from the complex interactions between the ejected photoelectron and electrons surrounding the absorbing atom. These oscillations are characteristic of the surrounding atoms and their distances from the absorbing atom, since varying distances will result in different backscattering paths, giving different wave interactions.



Above: When an X-ray photon is absorbed by an atom, it can ionize, giving off a photoelectron.



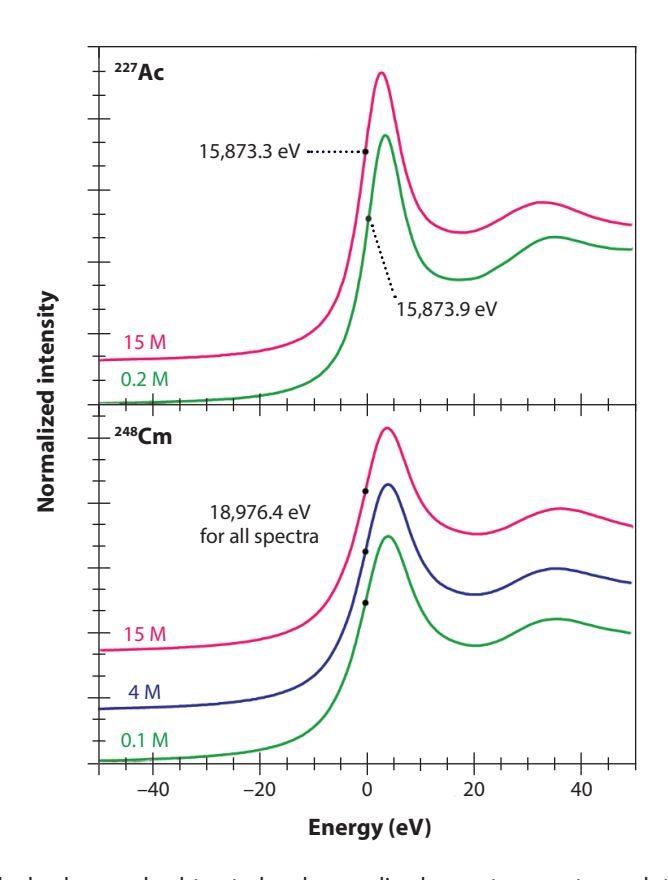


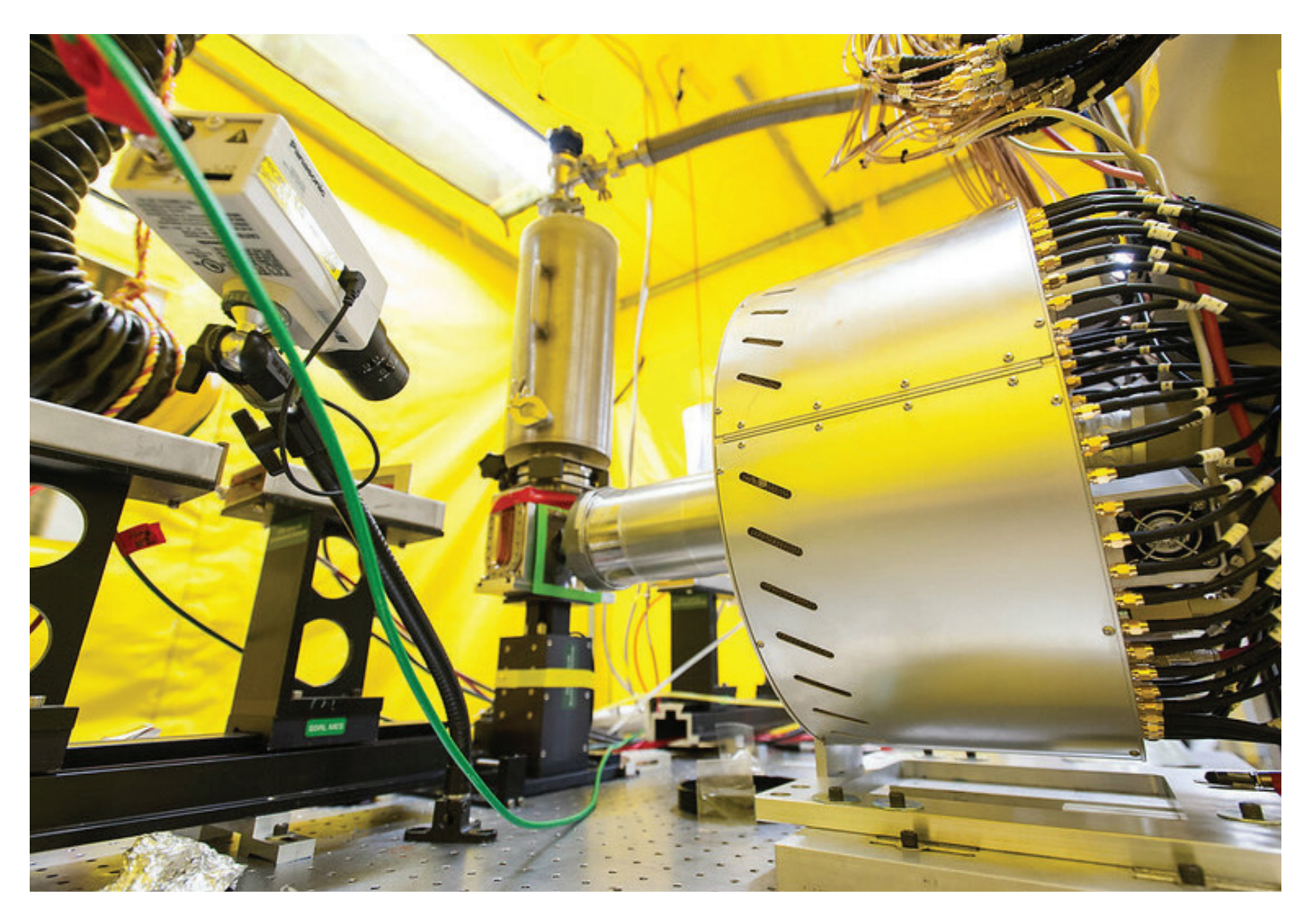
Figure 3. The background-subtracted and normalized room temperature solution-phase $An^{3+}L_3$ -edge XANES spectra from Ac^{3+} (top) dissolved in ammonium acetate-acetic acid (15 and 0.2 M, pH = 5.5) solutions and Cm³⁺ (bottom) dissolved in 15, 4, and 0.1 M solutions. Spectra are displayed with a slight y-offset for clarity. The dots show the inflection points.

• • •

of actinium and milligrams of americium and curium). In particular, while XANES is very sensitive to the oxidation state and coordination chemistry of the absorbing atom, EXAFS is useful for determining distances, coordination number, and species of the neighbors of the absorbing atom. Fig. 2 displays a cartoon representation of the interactions that occur between the analyte and its neighboring atoms. All of the X-ray absorption spectroscopy measurements were performed at the Stanford Synchrotron Radiation Lightsource, beamline 11-2, which is optimized for challenging X-ray measurements such as those with dilute or radioactive samples.

XANES results

The L_3 -edge XANES spectra in all three acetate solutions (dilute, intermediate, and concentrated) were dominated by an absorption peak superimposed on an absorption edge for both elements (Fig. 3). The inflection point for actinium(III) in dilute acetate solution was higher than the value recorded in concentrated solution (15,873.9 versus 15,873.3 eV) and an even greater difference was observed between it and the previously reported aquo ion (15,874.3 eV). We did not see this for curium. Instead, the curium(III) inflection points from all three acetate solutions were identical to the value previously determined for the aqua ion in dilute nitric acid. It is unclear why the actinium inflection points are more sensitive to ligand environments than curium, although one possible explanation is that they derive from more substantial orbital mixing in the actinium-ligand bonds (see p29 for a description of the relationship of actinide atomic number and interatomic bonding).



Beamline 11-2 at the Stanford Synchrotron Radiation Lightsource (SSRL) is a high-flux X-ray absorption spectroscopy (XAS) station dedicated to molecular biogeochemical and interface sciences. It is optimized for challenging XAS measurements on dilute or radioactive samples and interfaces. Credit: SSRL.

XANES alone did not offer substantial insights, as it is only sensitive to the oxidation state and electronic structure of the absorbing atom. Therefore, we turned to EXAFS to help determine the structure around the absorbing atom.

EXAFS results

For dilute acetate solutions, structural metrics from the actinium(III) L_3 -edge EXAFS data spectra were consistent with $Ac(H_2O)_9^{3+}$, equivalent to the two other literature reports and in agreement with predictions from molecular dynamics simulations. We also obtained a straightforward result for curium(III), as the data indicated eight coordinated water molecules, comparable to previous reports on the curium(III) aquo ion.

Concentrated solutions were, however, distinct from dilute, giving EXAFS spectra that were inconsistent with a single-ligand environment. Instead, multiple contributions associated with actinide-bound acetate were present (Fig. 4). For actinium,

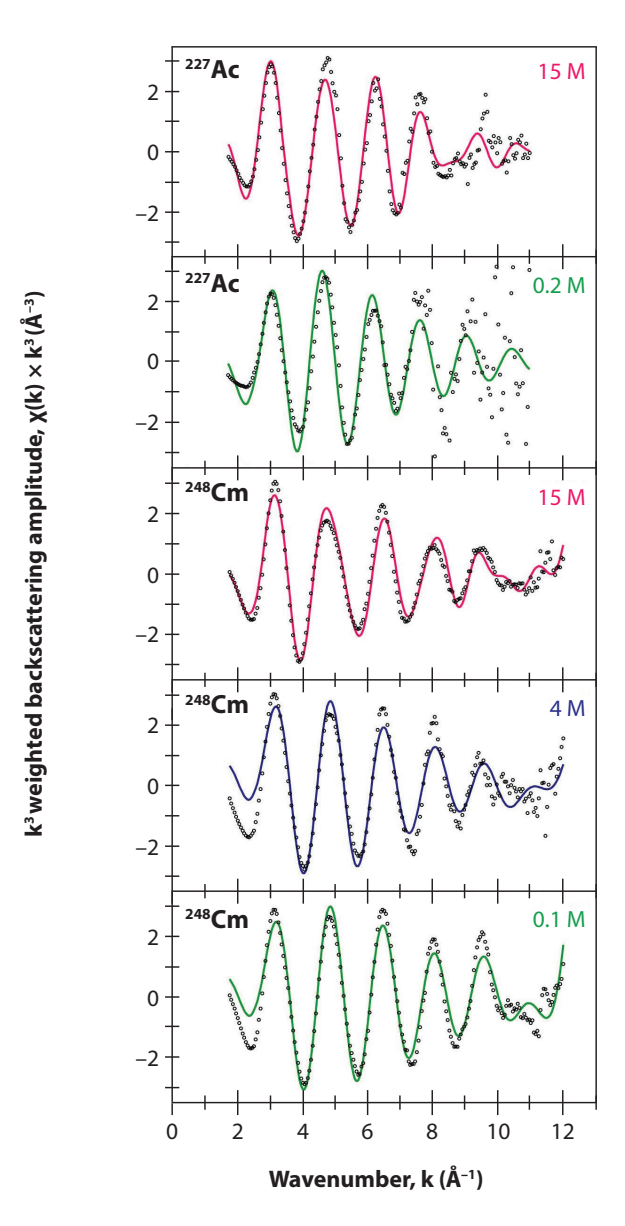
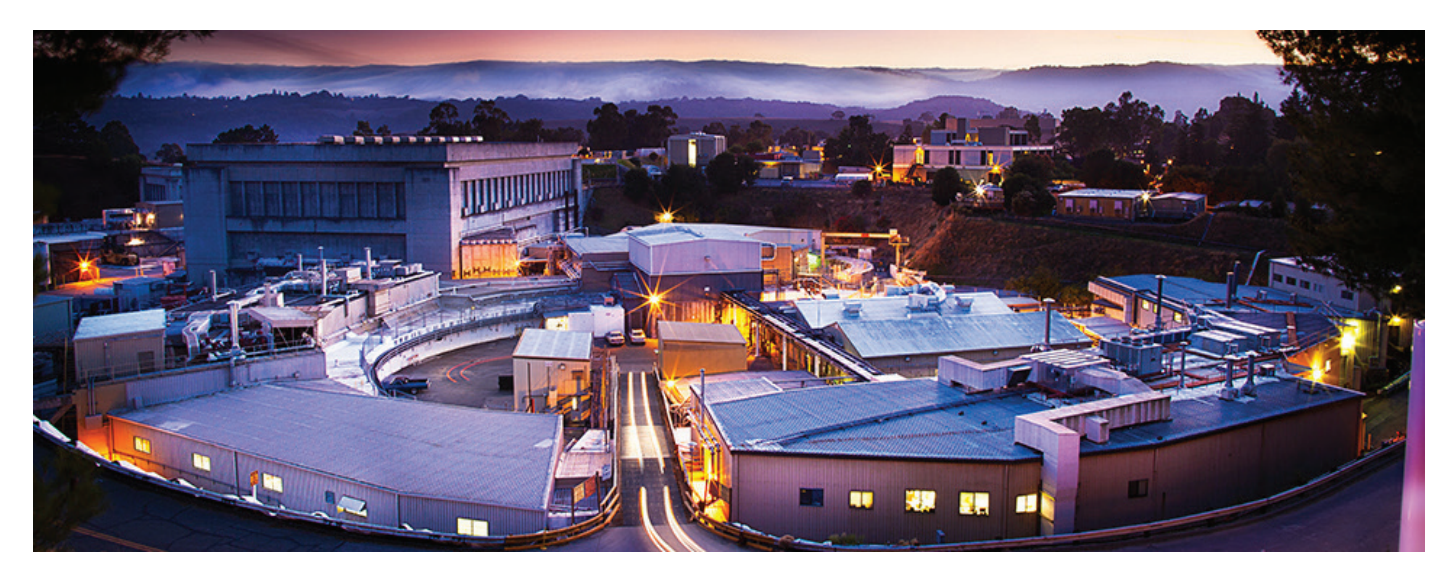


Figure 4. k^3 -weighted room temperature Ac^{3+} and Cm^{3+} L_3 -edge EXAFS spectra displaying the $\chi(k)$ function (points) with non-linear curve fitting (lines) from Ac^{3+} dissolved in ammonium acetate-acetic acid (15 and 0.2 M, pH = 5.5) solutions and from Cm^{3+} dissolved in 15, 4, and 0.1 M solutions. (N.B., k^3 -weighting reduces the contribution of light scattering atoms).

• • •

there were two well-resolved and short Ac–O scattering pathways in the innermost coordination sphere, corresponding to both water and acetate ligands. After carefully modeling the data, we found an average stoichiometry of six water molecules and three acetate ligands, i.e., $Ac(H_2O)_6(acetate)_3$.

For curium, the low-frequency contributions refined as a single environment of nine oxygen atoms. Longer-range electron scattering was modeled with 4.5 acetate ligands (to total nine oxygen donor atoms), giving Cm–O bond distances that were consistent with the X-ray diffraction data for nine-coordinate Cm(acetate)₅²⁻. Overall, these data suggest that the curium(III) inner coordination sphere is dominated by acetate in concentrated solutions, with minimal contributions from bound H₂O.



Aerial photograph of The Stanford Synchrotron Radiation Lightsource (SSRL) facility located in Menlo Park, CA.

Small changes in Lewis acidity impact actinide coordination chemistry

Our acetate studies align with the common assumption (and a limited number of experimental observations) that actinide(III) complexation is directly influenced by Lewis acidity (i.e., the strength of their attraction to electron donors). Curium, a stronger Lewis acid, showed an inner coordination sphere populated by approximately four acetate ligands in concentrated solutions where acetate ions were in high abundance. For the larger actinium cation, a weaker Lewis acid, the structure contained only three acetate ligands, formulated as neutral $Ac(H_2O)_6$ (acetate)₃.

This provides rare experimental data showing how 5*f*-element speciation varies as actinide ionic radii contract, analogous to behavior observed for rare earth elements. Although this is expected, the impact of the actinide contraction on coordination chemistry is scarce in the literature, likely due to the difficulties of handling these highly radioactive elements and performing detailed solution-state measurements. The implications of speciation differences in these acetate solutions are subtle but important. They highlight that the dominant species present in high-concentration solutions for the early actinides is not equivalent to that present for the minor actinides. We speculate that the increased complexation tendencies for the late actinide(III) cations likely persists even when the ammonium acetate-acetic acid concentration is less than 15 M. It seems possible that acetate prefers binding small *f*-elements (e.g., curium(III)) over large actinides (e.g., actinium(III)) between 4 and 15 M solution concentrations.

Summary

A range of X-ray absorption spectra were collected for actinium(III) and curium(III) in aqueous, buffered solutions of ammonium acetate-acetic acid at three different concentrations relevant to current laboratory applications. At low concentrations, the structures were found as the known aquo ions, $Ac(H_2O)_9^{3+}$ and $Cm(H_2O)_8^{3+}$. At high concentrations, where acetate ions are abundant, the actinium species was characterized as neutral $Ac(H_2O)_6$ (acetate)₃, whereas the curium solution showed an inner coordination sphere populated by approximately four acetate ligands. This increased affinity is likely due to the higher Lewis acidity of the curium(III) ion, which has a smaller ionic radius.

Actinide Research Quarterly

Better characterization of these aspects of aqueous actinide coordination chemistry would provide researchers with critical information about how active species in solution change with conditions, potentially having significant impact. We hope that this work motivates further study of actinides in relevant aqueous solutions.

Acknowledgments

Many thanks to Maryline G. Ferrier, Benjamin W. Stein, Laura M. Lilley, Stosh A. Kozimor, Maksim Y. Livshits, David H. Woen, Elodie Dalodière, Veronika Mocko, Frankie D. White, Karah E. Knope, Brian L. Scott, and Jennifer N. Wacker for their contributions. These contributions included project conceptualization, writing, editing, acquisition of XAS data, single crystal structure refinement, actinide purification, and optical measurements. We also thank the U.S. Department of Energy, Office of Science, Office of Basic Energy Sciences, Heavy Element Chemistry program (2020LANLE372) and LANL's LDRD-DR (20180005DR and 20190364ER). Postdoctoral support was provided by the Glenn T. Seaborg Institute. Use of the Stanford Synchrotron Radiation Lightsource, SLAC National Accelerator Laboratory, was supported by the U.S. DOE, Office of Science, Office of Basic Energy Sciences under Contract No. DE-AC02-76SF00515.

Further reading:

- Z.R. Jones, M.Y. Livshits, F.D. White, E. Dalodiere, M.G. Ferrier, L. M. Lilley, K.E. Knope, S.A. Kozimor, V. Mocko, B.L. Scott, B.W. Stein, J.N. Wacker, F.D. White, "Advancing understanding of actinide (III) (Ac, Am, Cm) coordination chemistry in ammonium acetate and acetic acid buffered aqueous stock solutions," Chem. Sci., 2021, 12, 5638.
- 2. M.G. Ferrier, B.W. Stein, S.E. Bone, S.K. Cary, A.S. Ditter, S.A. Kozimor, J.S. Lezama Pacheco, V. Mocko, G.T. Seidler, "The coordination chemistry of CmIII, AmIII, and AcIII in nitrate solutions: an actinide L3-edge EXAFS study," Chem. Sci., 2018, 9, 7078.
- 3. M.G. Ferrier, B.W. Stein, E.R. Batista, J.M. Berg, E.R. Birnbaum, J.W. Engle, K.D. John, S.A. Kozimor, J.S. Lezama Pacheco, L.N. Redman, "Synthesis and characterization of the actinium aquo ion," ACS Cent. Sci., 2017, 3, 176.



Actinide Research Quarterly is published by Los Alamos National Laboratory and is a publication of the Glenn T. Seaborg Institute for Transactinium Science, a part of the National Security Education Center. ARQ (est. 1994) highlights research in actinide science in such areas as process chemistry, metallurgy, surface and separation sciences, atomic and molecular sciences, actinide ceramics and nuclear fuels, characterization, spectroscopy, analysis, and manufacturing technologies.

LA-UR-25-20312

Address correspondence to:

Actinide Research Quarterly c/o Editor Mail Stop T-001 Los Alamos National Laboratory Los Alamos, NM 87545

ARQ can be read online at:

www.lanl.gov/arq

If you have questions, comments, suggestions, or contributions, please contact the ARQ staff at: arq@lanl.gov

National Security Education Center David L. Clark, Director

G. T. Seaborg Institute for Transactinium Science Science Advisors

Franz Freibert, Director Ping Yang, Deputy Director

> Editor Owen Summerscales

Designers/Illustrators Jacob Hassett Owen Summerscales

 $Los Alamos \ National \ Laboratory \ is \ operated \ by \ Triad \ National \ Security, \ LLC, \ for the \ National \ Nuclear \ Security \ Administration \ of \ U.S. \ Department \ of \ Energy \ (Contract \ No. \ 89233218CNA000001).$

This publication was prepared as an account of work sponsored by an agency of the U.S Government. Neither Triad National Security, LLC, the U.S. Government nor any agency thereof, nor any of their employees make any warranty, express or implied, or assume any legal liability or responsibility for the accuracy, completeness, or usefulness of any information, apparatus, product, or process disclosed, or represent that its use would not infringe privately owned rights. Reference herein to any specific commercial product, process, or service by trade name, trademark, manufacturer, or otherwise does not necessarily constitute or imply its endorsement, recommendation, or favoring by Triad National Security, LLC, the U.S. Government, or any agency thereof. Los Alamos National Laboratory strongly supports academic freedom and a researcher's right to publish; as an institution, however, the Laboratory does not endorse the viewpoint of a publication or guarantee its technical correctness.

Actinide Research Quarterly

Mail Stop T001 Los Alamos National Laboratory Los Alamos, NM 87545

arq@lanl.gov

Presorted Standard U.S. Postage Paid Albuquerque, NM Permit No. 532





